

A NEW TECHNIQUE FOR METAL OXIDE SURGE ARRESTERS FAILURE
DIAGNOSTIC USING RETURN VOLTAGE MEASUREMENT

ZULKURNAIN BIN ABDUL MALEK

RESEARCH VOTE NO:

78228

FAKULTI KEJURUTERAAN ELEKTRIK
UNIVERSITI TEKNOLOGI MALAYSIA

2009

ACKNOWLEDGEMENT

The author would like to acknowledge and thank Ministry of Higher Education for providing the grant for this research.

ABSTRACT

Due to their reliability and accuracy, many modern diagnostics based on dielectric voltage response, such as polarization/depolarization current (PDC), voltage decay (VD) and return voltage (RV) measurements, have been used in monitoring ageing processes of metal oxide (MO) varistors, which is the main part of a surge arrester. Among these diagnostics, recently, RV measurement (RVM) seems to be an increasingly popular method as it has high sensitivity to the condition of varistors and low sensitivity to disturbances in vicinity of the field measurements. Nonetheless, the basic interpretation based on the RVM essential parameters – peak RV, time-to-peak RV and initial slope of RV - provides insufficient information of the MO varistors condition since they are inevitably dependent on the measuring parameters such as the charging and discharging times as well as the test object temperature. Hence, this project focuses on a new way in interpreting the RVM parameters based on dielectric time constants analysis using an equivalent circuit of varistor microstructure, namely the Maxwell-Model. In order to investigate the ageing processes of MO varistors, two types of accelerated degradation techniques – impulse and heat degradations – are systematically conducted on test samples. Experimental results are presented and discussed in detail according to the underlying physical mechanism. On the basis of this concept, a sensible ageing parameter, *p-factor*, is used for better characterization of the ageing status of varistors.

KEYWORDS: Metal oxide varistor, surge arrester, ageing, degradation, return voltage measurement, dielectric time constant

ABSTRAK

Disebabkan oleh keboleharapan dan ketepatannya, banyak diagnostik moden berdasarkan pada respon voltan dalam dielektrik, seperti pengukuran pengutuban/penyahkutuban arus (PDC), voltan penyusutan (VD) dan voltan balikan (RV), telah digunakan dalam proses pemantauan penuaan varistor oksida logam (MO) yang merupakan binaan utama penangkap pusuan. Di antara diagnostic-diagnostik ini, kini, pengukuran RV (RVM) semakin meningkat digunakan kerana mempunyai kepekaan yang tinggi terhadap keadaan varistor dan sensitiviti rendah terhadap gangguan persekitaran proses pengukuran. Walaubagaimanapun, penguraian asas berdasarkan pembolehubah penting RVM - puncak RV, masa-ke-puncak RV dan kecerunan awal RV - tidak memberi maklumat yang cukup tentang keadaan varistor MO kerana ia bergantung pada parameter pengukuran seperti tempoh pengecasan and penyahcasan serta suhu objek. Oleh kerana itu, projek ini fokus pada cara baru dalam mengurai pembolehubah RVM berdasarkan analisis pemalar dielektrik masa dengan menggunakan litar yang sesuai untuk varistor mikrostruktur - Maxwell-Model. Dalam proses untuk menyiasat penuaan varistor MO, dua jenis teknik penuaan – secara aplikasi dedenyut dan pemanasan - dilakukan secara sistematik pada sampel. Keputusan eksperimen tersebut dilaporkan dan dibincangkan secara terperinci sesuai dengan mekanisma fizikal yang mendalam. Atas dasar konsep ini, pembolehubah yang sesuai, *p-faktor*, digunakan untuk menggambarkan dengan lebih baik status penuaan varistor.

TABLE OF CONTENTS

| CHAPTER | TITLE | PAGE |
|----------|---|----------|
| | ACKNOWLEDGEMENT | iv |
| | ABSTRACT | v |
| | ABSTRAK | vi |
| | TABLE OF CONTENTS | vii |
| | LIST OF TABLES | x |
| | LIST OF FIGURES | xi |
| | LIST OF SYMBOLS | xiii |
| | LIST OF ABBREVIATIONS | xv |
| 1 | INTRODUCTION | 1 |
| | 1.1 Project Background | 1 |
| | 1.2 Problem Statement | 2 |
| | 1.3 Objective of Project | 3 |
| | 1.4 Scope of Project | 3 |
| | 1.5 Report Outline | 3 |
| 2 | LITERATURE STUDY | 5 |
| | 2.1 ZnO Varistor as Overvoltages Protective Device | 5 |
| | 2.1.1 Introduction | 5 |
| | 2.1.2 Microstructure and Common Equivalent Circuit of ZnO Varistor | 6 |
| | 2.1.3 Electrical Characteristics of ZnO Varistor | 7 |
| | 2.1.4 Principle of Operation of ZnO Varistor | 8 |
| | 2.2 Degradation and Failure Mode of ZnO Varistor | 9 |

| | | |
|----------|--|-----------|
| 2.2.1 | Electrical and Thermal Stresses | 10 |
| 2.2.2 | Failure Mode | 11 |
| 2.3 | ZnO Varistor Diagnostic Technique using Return Voltage Measurements Method | 11 |
| 2.3.1 | Introduction | 11 |
| 2.3.2 | Return Voltage Measurements as a Reliable Diagnostic Technique for ZnO-based Protective Device | 12 |
| 2.3.2.1 | Basics of Return Voltage Measurements Phenomenon | 12 |
| 2.3.2.2 | Previous Researches of Return Voltage Measurements on Insulation System | 14 |
| 3 | METHODOLOGY | 16 |
| 3.1 | Modeling ZnO Varistor based on Return Voltage Measurements Phenomenon | 16 |
| 3.1.1 | Common Model of ZnO Varistor | 16 |
| 3.1.2 | Modeling ZnO Varistor based on Maxwell- Model | 17 |
| 3.1.3 | Evaluation of Maxwell-Model Circuit | 18 |
| 3.2 | Laboratory Studies on ZnO Varistor Degradation | 20 |
| 3.2.1 | Test Sample Selection | 20 |
| 3.2.2 | Return Voltage Measurements | 22 |
| 3.2.3 | Total Leakage Current Measurements | 24 |
| 3.2.3 | 1 mA Reference Voltage Measurements | 26 |
| 3.2.4 | Artificial Degradation of ZnO Varistor | 27 |
| 3.2.4.1 | Impulse Degradation | 27 |
| 3.2.4.2 | Heat Degradation | 30 |
| 3.3 | Interpretation of Return voltage Measurements | 31 |
| 3.4 | Project Flow Chart | 32 |
| 4 | DATA AND DISCUSSION | 34 |
| 4.1 | Introduction | 34 |

| | | |
|----------|--|-----------|
| 4.2 | Results of Return Voltage Measurements | 34 |
| 4.2.1 | Sample A – Impulse Degradation | 34 |
| 4.2.2 | Sample B – Heat Degradation | 36 |
| 4.2.3 | Sample C – Impulse Degradation | 38 |
| 4.2.4 | Sample D – Heat Degradation | 40 |
| 4.3 | Results of Total Leakage Current Measurements | 42 |
| 4.4 | Results of 1 mA Reference Voltage Measurements | 44 |
| 4.5 | Results Comparison | 45 |
| 5 | CONCLUSION & SUGGESTION | 48 |
| 5.1 | Conclusion | 48 |
| 5.2 | Suggestion | 49 |
| | REFERENCES | 50 |
| | Appendices A - C | 54 |

LIST OF TABLES

| TABLE NO. | TITLE | PAGE |
|------------------|--|-------------|
| 3.1 | Specifications of Samples | 21 |
| 3.2 | Artificial Degradation Works for All Samples | 27 |
| 4.1 | Results of Total Leakage Current Measurements | 43 |
| 4.2 | Results of 1 mA Reference Voltage Measurements | 44 |
| 4.3 | Results Comparison between RVM, Total Leakage Current and 1 mA Reference Voltage Measurements | 46 |

LIST OF FIGURES

| FIGURE NO. | TITLE | PAGE |
|------------|--|------|
| 2.1 | Microstructure of ZnO Material | 6 |
| 2.2 | Simple Equivalent Circuit of ZnO Material | 7 |
| 2.3 | Typical V-I Characteristics Curve of MO Varistor on a Linear Scale, using Sample from Manufacturer | 8 |
| 2.4 | MOV Operation (a) Under Normal Operating Voltage and (b) Under Overvoltage Condition | 9 |
| 2.5 | Arrangement of Return Voltage Measurement | 13 |
| 2.6 | Return Voltage Cycle | 13 |
| 3.1 | Common Equivalent Circuit of ZnO Material for RVM Phenomenon | 17 |
| 3.2 | Maxwell Equivalent Circuit for ZnO Material | 18 |
| 3.3 | Voltages across the capacitors C_1 and C_2 (Figure 3.2) during RVM | 19 |
| 3.4 | (a) Block-type, and (b) Radial Leaded-type Varistors | 20 |
| 3.5 | Automatic Recovery Voltage Meter Type RVM5462 | 23 |
| 3.6 | Experimental Setup of RV Measurements | 23 |
| 3.7 | Circuit Diagram of RV Measurements | 24 |
| 3.8 | Experimental Setup of Total Leakage Current Measurements | 25 |
| 3.9 | Circuit Diagram of Total Leakage Current Measurements | 25 |
| 3.10 | Computer-Connected Picoscope | 25 |
| 3.11 | Voltage and Current Waveforms of a Sample During 1 mA Reference Voltage Measurement | 26 |
| 3.12 | Combination Impulse Waveshapes Generator, HAEFELY PSURGE30 | 28 |

| | | |
|------|--|----|
| 3.13 | Impulse Degradation Experimental Setup | 29 |
| 3.14 | An example of Lightning Combination Oscillograms Used for Impulse Degradation | 29 |
| 3.15 | Digimatic Drying Oven | 30 |
| 3.16 | Relationship Between p -factor and λ | 32 |
| 3.17 | Flow Chart of Project | 33 |
| 4.1 | Peak RV, RV Initial Slope and Time-to-Peak RV Plots For Sample A | 35 |
| 4.2 | Relationship Between p -factor and $\lambda=\tau_2/\tau_1$ for Sample A | 36 |
| 4.3 | Peak RV, RV Initial Slope and Time-to-Peak RV Plots For Sample B | 37 |
| 4.4 | Relationship Between p -factor and $\lambda=\tau_2/\tau_1$ for Sample B | 38 |
| 4.5 | Peak RV, RV Initial Slope and Time-to-Peak RV Plots For Sample C | 39 |
| 4.6 | Relationship Between p -factor and $\lambda=\tau_2/\tau_1$ for Sample C | 40 |
| 4.7 | Peak RV, RV Initial Slope and Time-to-Peak RV Plots For Sample D | 41 |
| 4.8 | Relationship Between p -factor and $\lambda=\tau_2/\tau_1$ for Sample D | 41 |
| 4.9 | Total Leakage Current Measurements for Sample D | 42 |
| 4.10 | Chart of Slope of Total Leakage Current Measurements for All Samples | 43 |
| 4.11 | Chart of 1 mA Reference Voltage Measurements for All Samples | 45 |
| 4.12 | Charts of Comparison for Each Technique for All Samples | 47 |

LIST OF SYMBOLS

| | | |
|-----------------|---|--|
| R_{IG} | - | Resistance of intergranular layers |
| C_{IG} | - | Capacitance of intergranular layers |
| R_{GRAIN} | - | Resistance of grains |
| I | - | Current |
| K | - | Ceramic constant |
| V | - | Voltage |
| α | - | Non-linearity exponent |
| $S1$ | - | Switch 1 |
| $S2$ | - | Switch 2 |
| U_p | - | Charging voltage |
| t_c | - | Charging time |
| t_d | - | Discharging time |
| U_m | - | Peak return voltage |
| t_m | - | Time to reach return voltage |
| s | - | Initial slope of return voltage |
| R_o | - | Geometric resistance |
| C_o | - | Geometric Capacitance |
| R_{ns} | - | Resistance of n-th parallel branches |
| C_{ns} | - | Capacitance of n-th parallel branches |
| ε_r | - | Relative permittivity |
| ρ | - | Specific resistance |
| τ_1 | - | Dielectric time constant of material 1 |
| τ_2 | - | Dielectric time constant of material 2 |
| C_1 | - | Capacitance of material 1 |
| C_2 | - | Capacitance of material 2 |
| ε_1 | - | Permittivity of material 1 |
| ε_2 | - | Permittivity of material 2 |

| | | |
|-------------|---|------------------------------------|
| R_1 | - | Resistance of material 1 |
| R_2 | - | Resistance of material 2 |
| ρ_1 | - | Specific resistance of material 1 |
| ρ_2 | - | Specific resistance of material 2 |
| R_L | - | Resistor of current limiter |
| V_{HV} | - | Voltage on high voltage arm |
| V_{LV} | - | Voltage on low voltage arm |
| $^{\circ}C$ | - | Degree Celsius |
| τ | - | Dielectric time constant |
| U_r | - | Return voltage |
| U_s | - | Voltage after short circuit period |
| p -factor | - | New ageing parameter |

LIST OF ABBREVIATIONS

| | | |
|---------|---|--|
| UTM | - | Universiti Teknologi Malaysia |
| IVAT | - | Institute of High Voltage and High Current |
| ZnO | - | Zinc oxide |
| MOV | - | Metal oxide varistor |
| MO | - | Metal oxide |
| MOSA | - | Metal oxide surge arrester |
| VD | - | Voltage decay |
| PDC | - | Polarization/Depolarization current |
| RV | - | Return voltage |
| RVM | - | Return voltage measurement |
| V-I | - | Voltage-current |
| DC | - | Direct current |
| MCOV | - | Maximum continuous operating voltage |
| rms | - | Root mean square |
| Hz | - | Hertz |
| mm | - | Millimeter |
| kA | - | Kilo amperes |
| kV | - | Kilo volts |
| μ s | - | Micro second |
| pF | - | Pico farad |
| J | - | Joule |

LIST OF APPENDICES

| APPENDIX | TITLE | PAGE |
|-----------------|--|-------------|
| A | Block-type Varistor Specifications | 54 |
| B | Radial Leaded-type Varistor Specifications | 55 |
| C | Printed Results from RVM 5462 | 56 |

CHAPTER 1

INTRODUCTION

1.1 Project Background

Surge protection devices are often used to protect power and electronic equipment from the destructive transient overvoltage from lightning or other large-magnitude surge. These devices are used to limit the overvoltage to a level which is sufficiently safe for the equipment being protected by diverting the large current to ground. The non-linearity characteristics of these devices depend on their material composition. One type of non-linear devices is known as metal oxide varistor (MOV). MOV is a ceramic device with highly non-linear electrical characteristics; similar to those of a back-to-back diode, and has been used for low voltage application (below 1 kV). For higher voltage application that is above 1 kV the protection device is usually known as metal oxide surge arrester (MOSA) which may consists of several MOV blocks. Due to its high nonlinear characteristics, these devices have high energy absorption capability which is a good characteristic for an overvoltage suppressor.

However, these nonlinear characteristics can be degraded by the effects of electrical and thermal stresses as well as chemical reactions with the surrounding material. Usually, the thermal stress is considered as effect due to the temperature rise of the metal oxide materials subsequent to the discharge of high energy surges. While, the electrical stress may be the effects of voltage stress by its own operating

voltage at ambient temperature or by high current stress due to overvoltages occurrence.

In the past, many investigations of several non-destructive diagnostic techniques have been conducted for reliable condition assessment of the ageing of MOSA. These diagnostic techniques include the standard 1mA reference voltage, lightning impulse discharge residual voltage, voltage decay (VD), polarization or depolarization current (PDC) and Return Voltage (RV) measurements. The modern diagnostic techniques based on dielectric response such as VD, PDC and RV measurements, have also been used to evaluate insulating materials such as cables and transformers [1-4].

Among these modern diagnostic techniques, recently, the return voltage measurement (RVM) seems to be increasingly used as a reliable diagnostic method in monitoring the ageing process of the metal oxide materials due to its high sensitivity to smaller degrees of degradation [5]. In addition, RVM has low sensitivity to disturbances by external noise, a situation that is auspicious for in-field measurements [6].

1.2 Problem Statement

RVM method is a good approach to attain the information of insulating components condition for devices such as ZnO varistor (under normal operating mode). Due to less sensitive to disturbances, the measurements are reliable and also reproducible, at least with regard to the collection of the data. Unfortunately, in the past, not all RVM interpretation methods suggest correct insulation components condition information because of unreliable diagnosis parameters and inaccurate RVM data interpretation approach. Hence, this project focus on investigation of an accurate and correct way to interpret RVM data of ZnO varistor in order to obtain real physical condition of the ZnO insulation.

1.3 Objective of Project

There are two main objectives that have been achieved in this project:

- To model the equivalent circuit of ZnO varistor according to RVM phenomenon using Maxwell multilayer dielectric circuit.
- To investigate reliable interpretation of ZnO degradation process using RVM method.

1.4 Scope of Project

The main scope of this project is to study the diagnostic technique of ZnO varistor based on RVM method which includes:

- Study of behaviour and characteristics of metal oxide material;
- Study of theory, principles and interpretation of RVM;
- Evaluation of metal oxide material using multilayer dielectric approach – Maxwell-Model;
- Experimental works of ageing investigation on MOV using RVM method; and
- Results validation by comparison with total leakage current and 1 mA reference voltage measurements.

1.5 Report Outline

This report is divided into five chapters. Generally, some basic principles, theories, equations, previous researches' references, experimental result and discussions are discussed included in these chapters based on the contents requirements of each chapter.

In chapter 1, the author has included the project overview and the main objectives of conducting this project. Chapter 2 presents some background information of the project, such as the description of ZnO varistor as overvoltage protective device, and RVM as ZnO varistor diagnostic technique. This chapter briefly explains the ZnO varistor structure, common equivalent circuit and electrical characteristics as well as the importance of conducting a research on its diagnostic technique. At the end of the chapter, the author summarizes the current research works done by other researchers and of course their valuable recommendations.

Chapter 3 presents the methodologies of modeling ZnO varistor as well as the experimental procedures of carrying out the RV measurements. These are presented in a flow chart form together with a brief explanation. The RVM interpretation methods are discussed at the end of this chapter. Then, data and discussion are covered in Chapter 4.

Finally, Chapter 5 summarizes all the works and studies that had been presented in the previous four chapters. Besides, some future works are suggested at the end of the chapter.

CHAPTER 2

LITERATURE STUDY

2.1 ZnO Varistor as Overvoltage Protective Device

2.1.1 Introduction

ZnO varistor plays an important role in avoiding any electrical or electronic equipment failure caused by dangerous, damaging transients or lightning surges. ZnO varistors are permanently connected from line to ground near the equipment being protected. Equipment failure can be minimized from better surge protection, that is highly desirable in order to promise good overall system reliability. The protection level of ZnO varistor depends on the withstand requirements such as high-energy absorption capability, current withstand and voltage withstand levels. A conventional varistor is an insulator or a very poor conductor at nominal operating condition so that it can prevent power follow current flowing through it. At the occurrence of a surge, it must be able to transform to a relatively good conductor (with some equivalent resistance) and diverting safely thousands of amperes of current to the ground. After the dissipation of surge current, a good varistor should return back to the non-conducting mode with its original V-I characteristics restored.

2.1.2 Microstructure and Common Equivalent Circuit of ZnO Varistor

MOV has highly non-linear resistance which is primarily zinc oxide added with other materials. Conductive zinc oxide grains separated by boundaries that form semiconductor junctions, just like a semiconducting diode. A metal oxide varistor microstructure is equivalent to combinations of millions series and parallel semiconducting diodes. Figure 2.1 shows the conduction mechanism in a metal oxide varistor. As shown in the figure, the electrical behaviour of the metal oxide varistor results from the number of microvaristors connected in series or in parallel. Energy absorbers are provided for each microvaristor in form of grains with optimum thermal contact which allow high absorption of energy and thus exceptionally high surge current capability [7]. The resistance is very high with low voltage across the boundaries and vice versa.

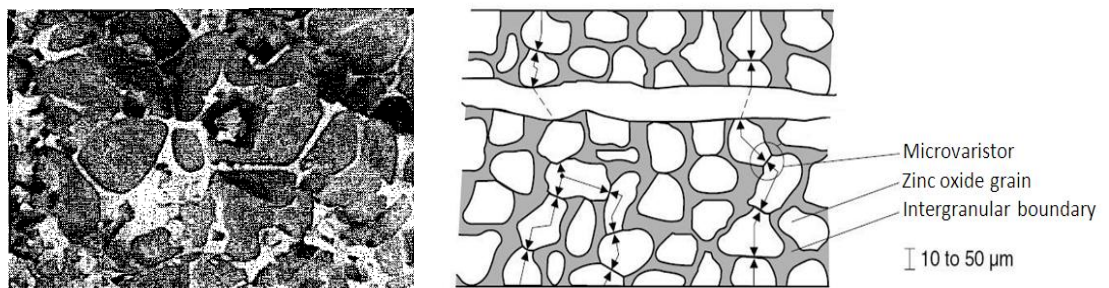


Figure 2.1 Microstructure of ZnO material

The simple equivalent model to describe the ZnO material in terms of electrical components is an R_{IG} - C_{IG} parallel circuit in series with another resistor, R_{GRAIN} and an inductance. R_{IG} is defined as a highly non-linear resistor with increasing voltage. Similar to non-linear behaviour of intergranular layers of ZnO material, we have the capacitance, C_{IG} . R_{GRAIN} is the resistance of conducting ZnO grains. The capacitance of ZnO grains is very small and can be neglected and the series inductance represents the inductance of the arrester body which is only considered for the steep response currents. The resulting equivalent circuit modelled is as shown in Figure 2.2 [8].

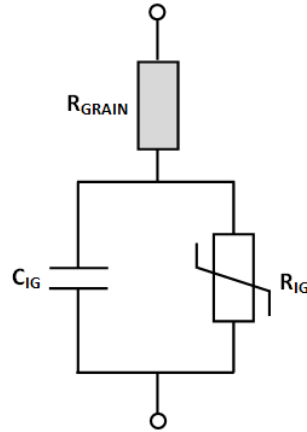


Figure 2.2 Simple Equivalent Circuit of ZnO Material

2.1.3 Electrical Characteristics of ZnO Varistor

ZnO material has high non-linear V-I characteristics and high energy absorption capability as their polycrystalline nature and the large number of intergranular barriers [9]. A typical V-I characteristics of a ZnO varistor on a linear scale can be seen in Figure 2.3. A reliable varistor must possess acceptable V-I characteristics at its original value during operation and after experiencing the electrical stresses resulting from surges. Approximately, the voltage dependence of varistor can be characterized as:

$$I = KV^\alpha$$

where,

I = current through varistor,

K = ceramic constant depending on varistor type,

V = voltage across varistor, and

α = non-linearity exponent of curve.

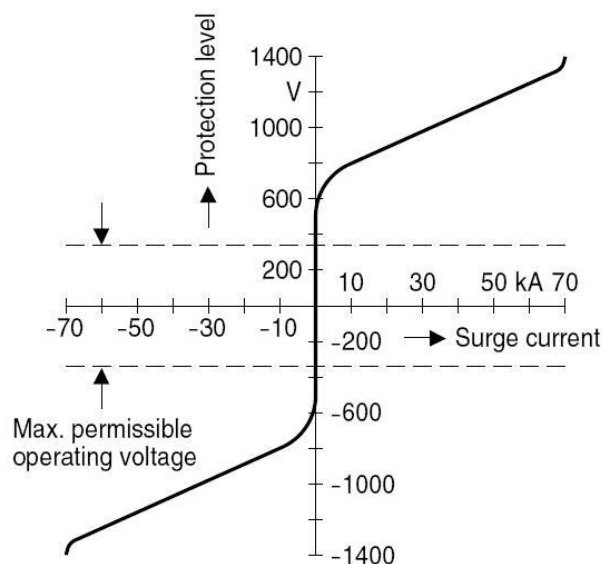


Figure 2.3 Typical V-I Characteristics Curve of MO Varistor on a Linear Scale, using Sample from a Manufacturer [7]

A V-I characteristic for a typical resistor is linear and has the value of $\alpha = 1$. Generally, as the value of α increased, the characteristics of the varistor are approaching the ideal one. For a modern design of varistor, typical range of the α value is between 30 and 100 [9].

2.1.4 Principle of Operation of ZnO Varistor

MOVs protect any equipment revealable to permanent damage from rapid, long term lightning strikes. They must be installed closely to the equipment being protected. Figure 2.4 shows the operation of MOV under normal operating voltage and under overvoltage condition. As shown in the figure, the MOV act as the protection component of the equipment. Under normal operation, MOV has very high impedance up to several mega ohms and it can be considered as open circuit. Therefore, all of the current in circuit will flow through the equipment and bypassing the MOV.

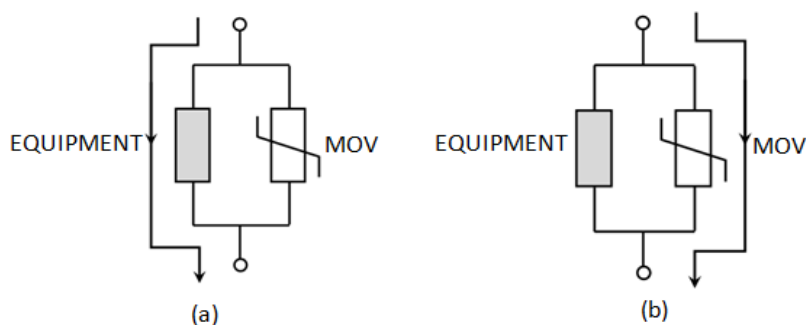


Figure 2.4 MOV Operation (a) Under Normal Operating Voltage and (b) Under Overvoltage Condition

When subjected to overvoltage, instantly, the impedance of the ZnO varistor declines to a few ohms or less for severe surges to avoid large current flows through equipment. After the surge absorption is completely done, immediately the varistor returns to its normal high impedance and restores its original characteristics. Non-linear characteristics would eliminate the power follow current flowing through it after the surge was done. This is the main advantage of the varistor where its residual voltages at high currents can be reduced.

In addition, depending on protection levels and applications; there are various rating parameters of the varistor. Maximum continuous operating voltage (MCOV) is the most essential rating of a metal oxide varistor. MCOV is defined as the maximum designated rms value of power frequency voltage that may be applied continuously between the terminals of the varistor. The MCOV of the varistor must be above the normal upper limit on steady-state voltage. The rating of the varistor also depends on the possible temporary overvoltages [10].

2.2 Degradation and Failure Mode of ZnO Varistor

As mentioned before, a reliable ZnO varistor must possess acceptable V-I characteristics at its original value during usage and after experiencing the electrical stresses resulting from surges. However, these V-I characteristics may become

degraded due to various electrical stresses and environmental pollution. Consequently, monitoring the varistor condition becomes more complicated while in operation [10].

2.2.1 Electrical and Thermal Stresses

There are two factors that influence the degradation of MO varistor; thermal and electrical stresses. Typically, the thermal stresses are considered as effects of the solar radiation and pollution on the arrester housing and also due to the temperature rise of the MO element subsequent to the discharge of high energy surges. Meanwhile, the transient electrical stresses are accounted by the lightning, switching and temporary overvoltages effects [11].

It is believed that ion migration found a strong basis of existence based on the evidence of measurements of thermally stimulated currents of stressed MO varistors. The potential barrier height at MO grain is modified by charge migration due to the degradation of varistors. The charge migration is controlled by the varistor electric field and temperature.

From previous studies, it is known that degradation mainly affects the pre-breakdown region of the V-I curve and results in increased leakage currents. The degradation is concluded to be a grain boundary related phenomenon since the pre-breakdown region is grain boundary controlled. A stressed MO varistor also believed to change its microstructure when it is preheated to certain temperatures depending on its previous degree of degradation and resulting in the change in its capacitive and resistive characteristics [10].

2.2.2 Failure mode

The performance of varistor could be affected by rapid higher overvoltages activities throughout the time of their services. Damage on varistors can be seen as cracks on the MOV surface or defect surfaces resulting from stresses.

Before installing varistors to a system, one of essential considerations besides their rating, is the thermal effect, either due to environmental aspects or lightning surges. The temperature of varistors is increased with the ambient temperature or energy absorbed by them. This proliferation of temperature cause additional heat to the varistors. A phenomenon called thermal runaway takes place when the temperature exceeds the thermal capability of the metal oxide valve element.

Thermal runaway is a phenomenon that occurs whenever the MOV disc is exposed to elevated temperature during operation and begins to conduct – allow current flowing through it - at voltage below the rated clamping or switching voltage. Eventually, this phenomenon leads to physical destruction of the MOV component. Thus, some adequate laboratory tests on MOV performance are required to ensure good reliability of the varistor in service [12].

2.3 ZnO Varistor Diagnostic Technique Using RVM Method

2.3.1 Introduction

Since the degradation of ZnO varistors results in thermal runaway and leads to a short circuit, the condition evaluation of the ZnO insulation under normal operating voltage becomes significant to ensure their reliability in service. Several diagnostic techniques such as the standard 1mA reference voltage, lightning impulse discharge residual voltage, voltage decay (VD), polarization or depolarization current (PDC) and Return Voltage (RV) measurements, have been used to investigate the

insulation condition of ZnO varistors. Among these techniques, it has been proved that RVM technique is the most sensitive technique to detect smaller changes in ZnO insulation condition and furthermore it is insusceptible to field noises during the measurements [5, 6].

2.3.2 RVM Method as Reliable Diagnostic Technique for ZnO-based Protective Device

Since a few years back, RVM method is a favorable modern diagnostic technique for MO-based material since it sensitively detects smaller degrees of degradation. Due to its reproducibility, this method can also be used for on-site measurements [5]. Better assessment on the insulation performance, condition and degradation can be investigated and evaluated using this method.

2.3.2.1 Basics of RVM Phenomenon

Arrangement of RVM is shown in Figure 2.5. Based on the figure, with only switch S1 closed, RV measurement starts by charging a MO varistor with a DC voltage, U_p for a pre-selected time known as the charging time, t_c . This DC voltage must be much lower than the operating voltage of the varistor, so that the varistor is acting like an insulator. Next step is discharging the varistor by short circuiting both varistor's terminals to the ground for a short time period called the discharging time, t_d with switch S2 closed and switch S1 is opened. Finally, with switch S1 and S2 opened, the open circuit voltage that built up across the varistor is measured using an electrometer which is a high impedance measuring system. This build up voltage – the return voltage - is widely used to characterize the condition of the varistor being measured.

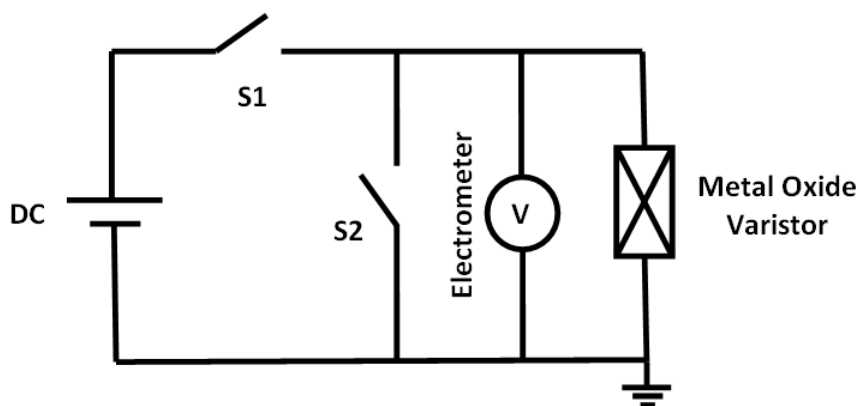


Figure 2.5 Arrangement of Return Voltage Measurements

Figure 2.6 shows the return voltage waveform for one cycle of measurement. U_p is the DC charging voltage and U_m is the peak return voltage after discharging. t_m indicates the time to peak of the return voltage. The initial slope of return voltage is denoted as s . These essential parameters - U_m , t_m and s - are widely used to evaluate the condition of insulation systems such as in varistors [1], surge arresters [5, 13, 14], cables [6, 15, 16] and power transformers [17].

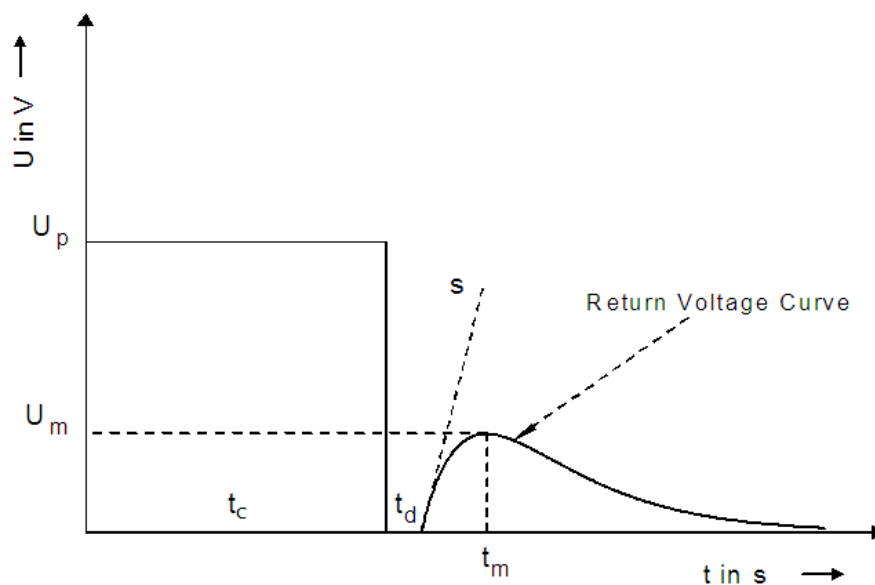


Figure 2.6 Return Voltage Cycle

2.3.2.2 Previous Researches of RVM on Insulation System

Previous findings [16, 18] found that the RVM method is a good tool to assess the condition of oil-paper insulation systems as it can provide a strong correlation between the progress of moisture content and ageing in the insulation and the polarization spectra. The ageing processes in paper-oil insulated high voltage cables and transformers can reliably be monitored by using this method due to its capability in detecting the changes in dielectric properties of composite insulations.

A reliable interpretation of correlation between the slope of the return voltage and period of ageing of the polymeric insulated cables, had also been proven [15]. As described in previous publications [5, 13, 14], the maximum U_m and the corresponding central time constant generally tend to decrease after a MO-based device experiences several current impulses. The effect of multipulse lightning current on MO material characteristics is claimed to be much more severe than single lightning pulse. Furthermore, the decrease in the central time constant maybe due to the increment of MO conductivity after undergoing ageing processes [14].

Since a ZnO varistor behaves almost like an insulator at normal operating voltage which is below its rated voltage, the polarization and depolarization of dipoles within the MO material as well as on the charging and discharging of grain boundaries and space effects can be monitored by RVM [5]. Therefore, RVM may be used as a good indicator for the ageing level of the MO. Yet, interpretation of the RVM data and results based on these three basic ageing parameters – U_m , t_m and s – suggested inaccurate condition of ZnO material since those parameters are influenced by DC charging voltage, U_p , charging time, t_c , discharging time, t_d and test object temperature [19] during the measurements.

Recently, the interpretation of RVM data has been studied and proven [6, 16, 20] to be a good indicator to insulation ageing such as in power cables based on dielectric time constant method using Maxwell dielectric equivalent circuit. This method seems plausible in monitoring the condition of the insulation system in

power cable which is a multi-layer insulation system – paper and oil – since it is independent from the U_p , t_c , t_d as well as surrounding temperature during the RV measurements. Based on the RV phenomenon, a physically adequate equivalent circuit of insulator has been developed to describe the insulation system and being used to deliver the accurate data about the dielectric properties which is a good indicator of ageing process. Since the ZnO structure consists of two different dielectric materials which are zinc oxide grain and intergranular layer, and behave as an insulator below its normal operating voltage, this interpretation method can be applied in evaluating the condition of the varistor.

CHAPTER 3

METHODOLOGY

3.1 Modelling ZnO Varistor based on RVM Phenomenon

3.1.1 Common Model of ZnO Varistor

In the past, the insulation of MO material under normal operating condition is commonly represented by an equivalent model consisting the insulation resistance, R_o and geometric capacitance, C_o with a number of additional R - C branches [21] as shown in Figure 3.1. The individual polarization process is represented by these R - C parallel branches with their time constant $R_{ns}C_{ns}$ and is treated independent to each other. The representation of the polarization processes using R - C parallel branches in line with the theory of distributed relaxation times to predict the response of the insulation, which hardly follows ideal Debye behaviour [21]. The displacement current in the insulation is determined by the geometric capacitance C_o , internal resistance R_o and the R - C pairs with the associated time constant and the conduction current is only by the internal resistance R_o .

Based on the equivalent circuit, a numerical fit approach is often used in the analysis of RV curves or polarization/depolarization currents over time. These numerical values, R_{ns} and C_{ns} , are calculated according to exponential fitting of the measured relaxation or depolarization current [21] and being used to characterize the condition of the ZnO varistor. However, these ‘*best fit*’ numerical values are only a purely formal description regardless of any physical meaning of ZnO insulation.

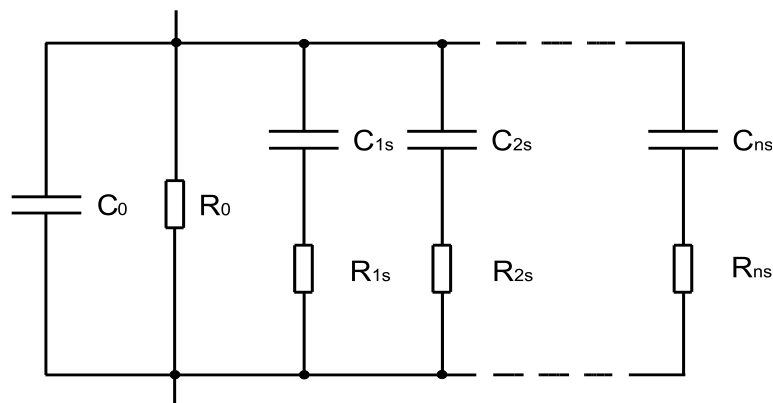


Figure 3.1 Common Equivalent Circuit of ZnO Material for RVM Phenomenon

3.1.2 Modelling ZnO Varistor Based On Maxwell-Model

As discussed in Section 2.1.2, the microstructure of ZnO varistor consists of two different dielectric properties - ZnO grains and intergranular layers - that is equivalent to combinations of millions series and parallel semiconducting diodes. Hence, as these dielectrics have different compositions with different relative permittivity, ϵ_r and specific resistance, ρ [8, 22], an adequate equivalent circuit for a ZnO varistor - multilayer dielectric - is the Maxwell-Model with two R - C parallel circuits in series as shown in Figure 3.2. The model is relevant to describe the boundary polarization process in the ZnO materials and more appropriate since it closely reproduces the real physical meaning of the condition of the ZnO material. Consequently, instead of only considering the molecular polarization processes during RV measurements, it also shows the phenomenon of boundary polarization which is primarily involving volume conductive processes.

When a multilayer dielectric is subjected to a DC voltage, which leads to a dielectric polarisation, capacitive voltage starts to distribute within both layers and continuously changes into a resistive voltage distribution. Electric charges migrate between layers and in part accumulate at interface boundaries, where local electric fields are generated by the charges to necessarily obey the continuity equation for the current density. After the charging voltage is removed, within the short circuit period, depolarisation of the insulation starts where the charges at the external

electrodes are released according to the dielectric layers time constants, $\varepsilon_1\rho_1$ and $\varepsilon_2\rho_2$. After this period, as the free charges have vanished, the dielectric depolarisation continues and results in the previous bound charges to become free charges. Consequently, a so-called ‘return voltage’ occurs across the multilayer dielectric due to the built-up of the free charges [23, 24].

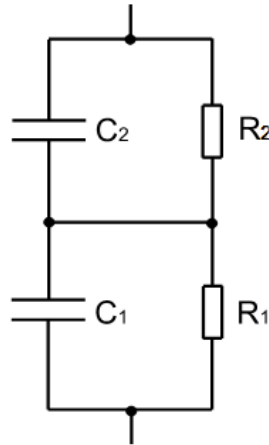


Figure 3.2 Maxwell Equivalent Circuit for ZnO Material

3.1.3 Evaluation of Maxwell-Model Circuit

Phenomenon of RV in a multilayer dielectric is analyzed on the basis of the Maxwell-Model [23] as shown in Figure 3.3. Referring to the figure, at the presence of DC voltage in multilayer dielectric during charging time, t_c , a capacitive voltage division of the DC charging voltage, U_p occurs between voltages across capacitor C_1 , U_1 , and capacitor C_2 , U_2 . Gradually, this capacitive voltage changes into an ohmic division according to resistances of R_1 and R_2 . Then, during short circuit period – discharging time, t_d – intermigration of charges take place, where both of the capacitors voltages decrease simultaneously with a time constant τ until these voltages are identical. After the short circuit is released, the voltages across both of the capacitors decrease independently depending on individual time constants, τ_1 and τ_2 , resulting in voltage build up, U_r across the dielectric.

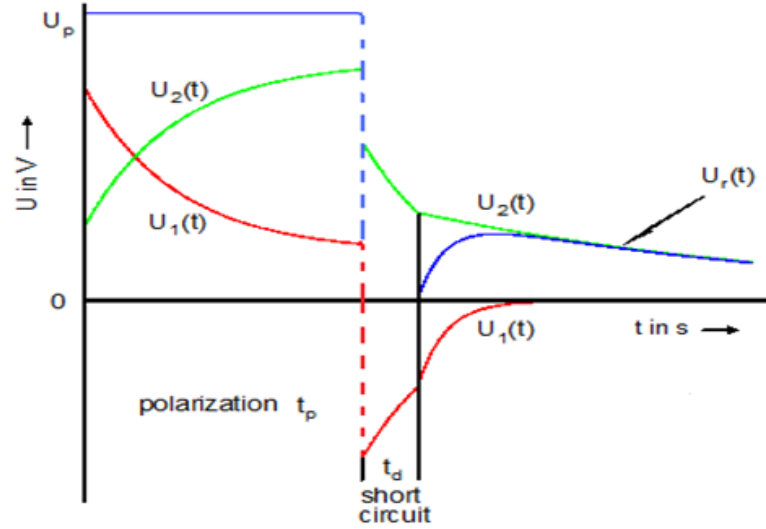


Figure 3.3 Voltages across the capacitors C_1 and C_2 (Figure 3.2) during RVM

For an insulation material, the dielectric time constant, τ is proportional to the product of relative permittivity, ϵ_r and the specific resistance, ρ , ($\epsilon_r\rho$) and it is independent of the geometrical dimensions and the shape of the dielectric [25]. The time constant is sensitively affected by any changes of ρ and ϵ_r [17]. Hence, for a parallel R - C circuit, the corresponding dielectric time constant, τ equals to RC ($\tau=RC$) where it exclusively determines the dielectric properties of the insulation.

For the equivalent circuit shown in Figure 8, the return voltage, U_r equation for a multilayer dielectric is given as,

$$U_r(t) = U_2(t) + U_1(t) = U_s \left(e^{-\frac{t}{\tau_2}} - e^{-\frac{t}{\tau_1}} \right)$$

$$\tau_2 = R_2 C_2$$

$$\tau_1 = R_1 C_1$$

The voltage across both of the capacitors after charging time, t_c and discharging time, t_d is as follows,

$$U_s = \frac{\lambda - 1}{1 + \lambda + \frac{R_2}{R_1} + \frac{C_2}{C_1}} U_p \left(1 - e^{-\frac{t_p}{\tau}} \right) e^{-\frac{t_d}{\tau}}$$

$$\tau = \frac{\tau_2 R_1 + \tau_1 R_2}{R_1 + R_2}$$

$$\lambda = \frac{\tau_2}{\tau_1} > 1$$

where τ is the time constant under short circuit of the dielectric system and λ is the dielectric constants ratio, τ_2/τ_1 . Obviously, return voltage equation, $U_r(t)$ has a complex dependence on U_s factor of the dielectric.

Based on the equations above, dielectric constant τ_2 is greater than τ_1 due to the dielectric properties of element R_1-C_1 is greater than element R_2-C_2 . For zinc oxide material, element R_1-C_1 represents the zinc oxide grains which are highly conductive component and element R_2-C_2 represents the intergranular layers, the non-conducting component.

3.2 Laboratory Studies on ZnO Varistor Degradation

3.2.1 Test Sample Selection

For experimental works in this project, two types of new ZnO varistor from different manufacturers were used. Two varistors from each manufacturer were chosen as project samples named as sample A, B, C and D. Sample A and B are block-type varistors while sample C and D are radial leaded-type varistors. Figure 3.4 shows the block-type and radial leaded-type varistors used in the project and details of these varistors are presented in Table 3.1. Full specifications of these varistors can be referred to Appendices A and B.



Figure 3.4 (a) Block-type, and (b) Radial Leaded-type Varistors

Table 3.1 Specifications of Samples

| Varistor Type | Block | Radial Leaded |
|---------------|--|---|
| Specification | Diameter: 40mm Height: 21mm Voltage Rating, AC: 3kV Current Rating: 10kA Max Continuous Operating Voltage: 2.55kV Voltage at 1mA: 4kV Lightning Impulse Residual Voltage at: 5kA - 8.3kV 10kA – 8.8kV 20kA – 10.3kV | Diameter: 14mm Voltage Rating, AC: 1000V Voltage Rating, DC: 1200V Peak Pulse Current at 8/20 μ s: 4.5 kA Max Clamping Voltage at 8/20 μ s: 2700V Max Transient Energy 10/1000 μ s: 220J Capacitance: 130pF Voltage at 1mA Max: 1800V Voltage at 1mA Min: 1425V |

In choosing the test samples, several characteristics of the devices must be considered in order to satisfy the experimental work requirements. Some characteristics of varistor are defined as follows:

- Maximum Continuous Operating Voltage (MCOV) - Maximum AC voltage applied continuously between the terminals of the varistor
- 1 mA Reference Voltage - Voltage required for 1 mA current flows through varistor
- Maximum Clamping Voltage – Maximum voltage across the varistor terminals when a lightning current impulse is applied
- Nominal Discharge Current – Peak value of lightning current impulse, which is used as varistor classification

- Energy Absorption Capability – Maximum level of energy subjected into varistor at which it can still cool down back to its normal operating temperature

3.2.2 Return Voltage Measurements

All the experimental works in this project were performed in the High Voltage Laboratory of the Institute of High Voltage and High Current (IVAT) in Universiti Teknologi Malaysia (UTM) Skudai. In this project, single cycle of RV measurements were conducted on each sample before and after experiencing degradation processes. Prior to any RV measurement, all test samples were firstly short circuited to ground for at least 24 hours to eliminate any remaining charges from previous tests. These previous effects normally influence the measurement accuracy and reproducibility [1].

The measurements of the return voltage were carried out using a commercial automatic recovery voltage meter, type RVM 5462 by TEXTEX Instruments, as shown in Figure 3.5. As described in Section 2.3.2.1, all the RVM processes including polarization (charging process), depolarization (discharging process), relaxation process and return voltage measurement, are automatically carried out by this portable microprocessor-controlled RVM meter. For each measurement, the essential parameters of RVM - U_m , t_m and s – were printed out (refer Appendix C) by its internal printer and the points of measured RV curves were recorded manually (not printable).

The settings of the RVM meter for each measurement can be referred as below:

| | |
|---------------------------|--|
| Charging DC voltage: | 500 V (Sample A and B) 200 V (Sample C and D) |
| Charging time, t_c : | 600 s |
| Discharging time, t_d : | 60 s |
| t_c/t_d ratio: | 10 |



Figure 3.5 Automatic Recovery Voltage Meter Type RVM 5462

In this project, the charging and discharging time ratio, t_c/t_d for RV measurements was not the same as previous researches, typically, t_c/t_d equal to 2 [1, 13, 14], 450 [19, 23] or 900 [20] due to the fact that the new essential RV curve parameter, p-factor (presented in Section 3.3), which is to be obtained by these procedures is independent from the t_c/t_d ratio [20]. The experimental setup of RV measurement is shown in Figure 3.6. Figure 3.7 shows the circuit diagram of the measurement. Referring to Figure 3.6, during the RVM, one terminal of the varistor is connected to the high voltage cable of the RVM meter (red crocodile clip) and another terminal is grounded (black crocodile clip).



Figure 3.6 Experimental Setup of RV Measurements

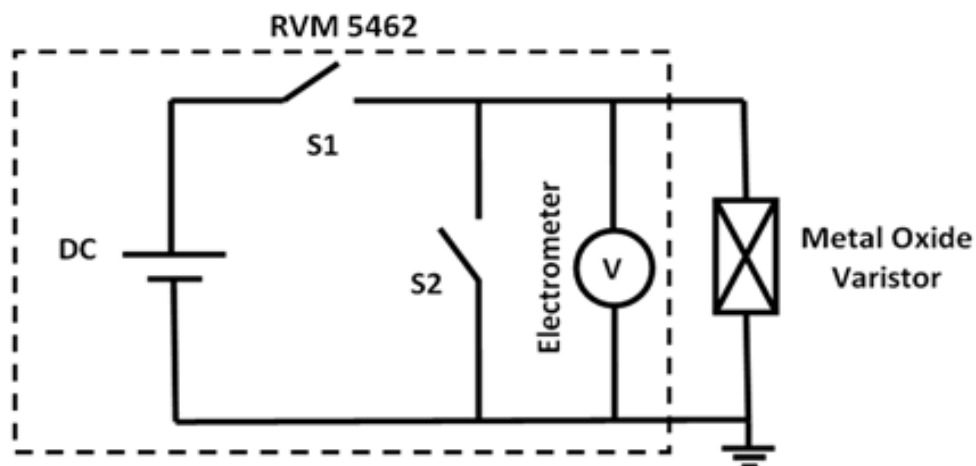


Figure 3.7 Circuit Diagram of RV Measurements

3.2.2 Total Leakage Current Measurements

The total leakage current method was used as one of the reference methods for RVM results justification. Comparison between these methods was discussed in detail in Chapter 4. The total leakage current measurements were performed for all test samples before and after each of degradation levels. The experimental setup and circuit diagram of the measurement can be respectively referred to in Figure 3.8 and Figure 3.9. The circuit consists of a step-up transformer, a resistance current limiter ($R_L = 10 \text{ M}\Omega$), a capacitive divider ($V_{HV}/V_{LV} = 5112$), a measuring resistance of $10 \text{ k}\Omega$ (resistive shunt) and a computer-connected Picoscope (refer Figure 3.10).

With the use of a Picoscope, for each sample, the rms value of total leakage current through the varistors was measured as the AC voltage source is increased gradually. These rms values of supply voltage and total leakage current were recorded and plotted. Detail discussions on the total leakage current measurements were presented in Chapter 4.



Figure 3.8 Experimental Setup of Total Leakage Current Measurement

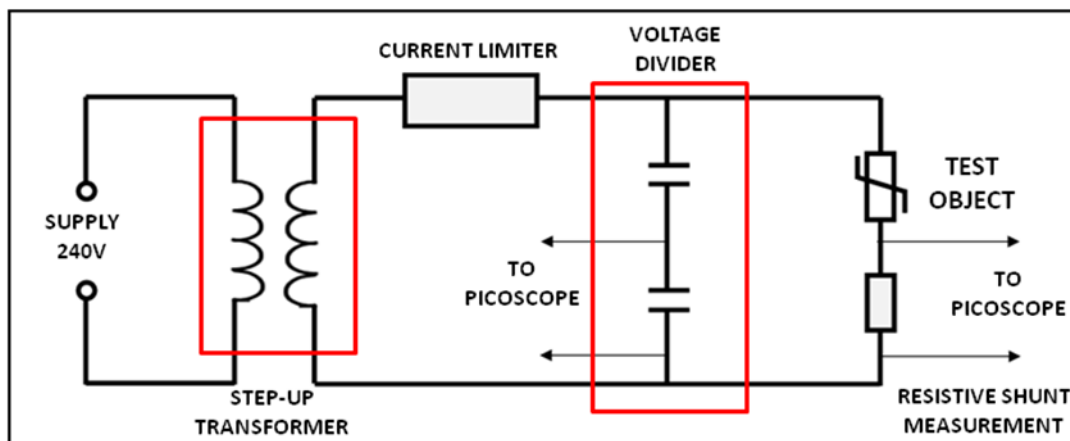


Figure 3.9 Circuit Diagram of Total Leakage Current Measurements



Figure 3.10 Computer-Connected Picoscope

3.2.3 1 mA Reference Voltage Measurements

The reference voltage is defined as the required voltage across varistor terminals to pass a specific reference current through it [26, 27]. Typically the reference current is in the range of 1 mA to 10 mA and rather close to the breakdown point in the breakdown region of the V-I characteristics. At this point, the total leakage current of the varistor consists of larger resistive component compared to the capacitive component. The resistive leakage current component is claimed to give significant changes in the change of the varistor characteristics due to ageing processes [28].

In this project, 1 mA of current flowing through the samples is also used as the reference current. Experimental setup for the 1 mA reference current measurement is similar to that for the total leakage current measurement as shown in Figure 3.8. However, the procedures on data collection were quite different. During each measurement, the voltage across the varistor is increased slowly until the value of total leakage current flowing through the varistor at the instant when the voltage is at its peak value, is equal to 1 mA (refer to Figure 3.11). This rms value of voltage, called as the reference voltage, is recorded. The effect of varistor degradation processes on the reference voltage was investigated in this project and is discussed in Chapter 4.

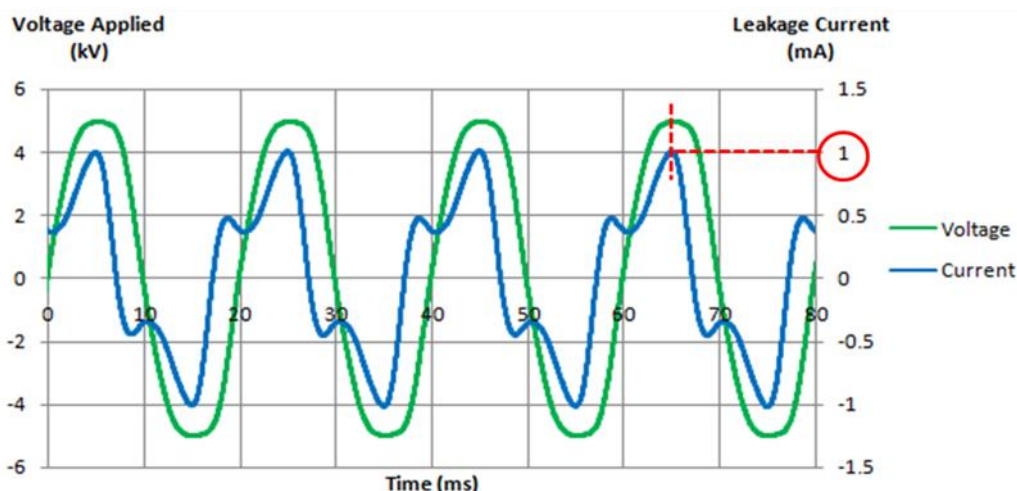


Figure 3.11 Voltage and Current Waveforms of a Sample during 1 mA Reference Voltage Measurement

3.2.4 Artificial Degradation of ZnO Varistor

There are two types of artificial degradation works that have been conducted on the samples in this project which are impulse and heat degradation techniques. All the degradation works are summarized in Table 3.2.

Table 3.2 Artificial Degradation Works for All Samples

| Degradation Technique | Sample | Degradation Level | Degradation Works for Each Level |
|-----------------------|--------|-------------------|---|
| Impulse | A | 1 st | 10 times 8.5kV-5kA Lightning Combination Wave at 1 min intervals |
| | | 2 nd | |
| | | 3 rd | |
| | C | 1 st | 5 times 3.6kV-2.5kA Lightning Combination Wave at 1 min intervals |
| | | 2 nd | |
| | | 3 rd | |
| Heat | B | 1 st | 120 hours / 5 days at 120°C |
| | | 2 nd | |
| | | 3 rd | |
| | D | 1 st | 120 hours / 5 days at 120°C |
| | | 2 nd | |
| | | 3 rd | |

3.2.4.1 Impulse Degradation

A combination wave generator of 1.2/50 μ s and 8/20 μ s lightning waveshapes, HAEFELY PSURGE30 (refer Figure 3.12), which is accessible in Institute of High Voltage & High Current (IVAT), was used for the impulse degradation works. Specifications of the combination waveshapes generator can be referred as below:

| | |
|-------------------------------|----------------------------------|
| Model: | HAEFELY Surge Generator PSURGE30 |
| Maximum energy: | 4.9 kJ |
| Open circuit output voltage: | 3-30 kV \pm 10 % |
| Voltage Front time: | 1.2 μ s \pm 30 % |
| Voltage Time to half value: | 50 μ s \pm 20 % |
| Short circuit output current: | 1.5-15 kA \pm 20 % |
| Current Front time: | 8 μ s \pm 20 % |
| Current Time to half value: | 20 μ s \pm 20 % |
| Dynamic impedance: | 2 Ω \pm 0.25 Ω |
| Impulse capacitor: | 9 μ F \pm 10 % |
| Impulse interval: | min. 10 s |

Sample A (block-type) and C (radial leaded-type) experienced three levels of impulse degradation. For sample A, each level consists of ten lightning combination impulses at 8.5 kV-5 kA with an interval of one minute. While, each degradation level of sample C consists of five lightning combination impulses at 3.6 kV-2.5 kA with one minute interval. The experimental setup of the impulse degradation is shown in Figure 3.13.



Figure 3.12 Combination Impulse Waveshapes Generator, HAEFELY PSURGE30

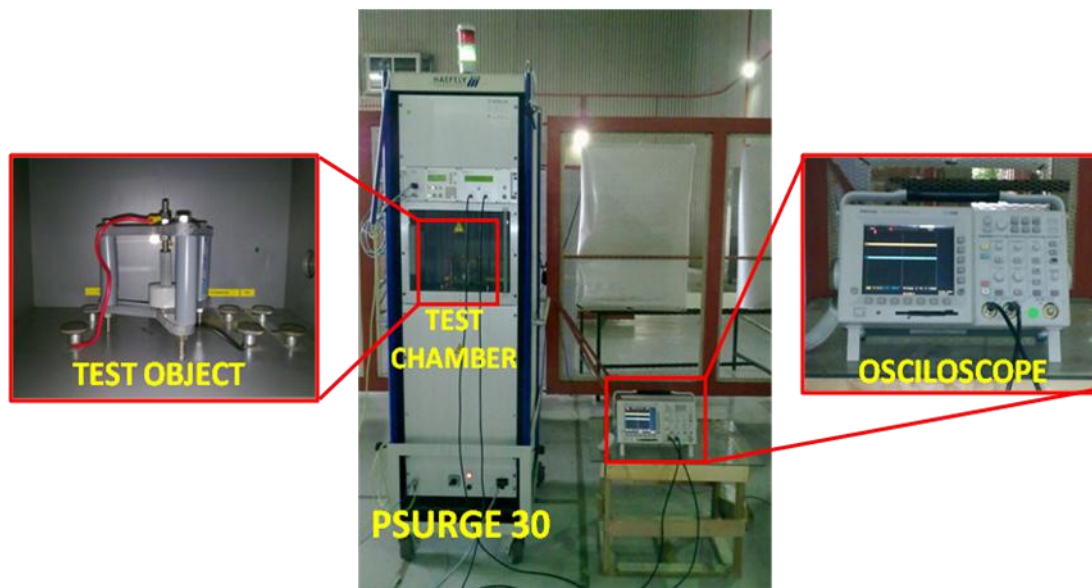


Figure 3.13 Impulse Degradation Experimental Setup

Referring to Figure 3.13, during the experiment, the varistor is located inside test object chamber of the combination waveshapes generator where one of the terminals is connected to the high voltage terminal of the combination waveshapes generator and the other one to the common terminal. For waveforms recording purpose, a digital storage oscilloscope is connected to the display unit of the combination waveshapes generator. An example of the oscillograms generated by the lightning combination waveshapes generator recorded by the oscilloscope is shown in Figure 3.14.

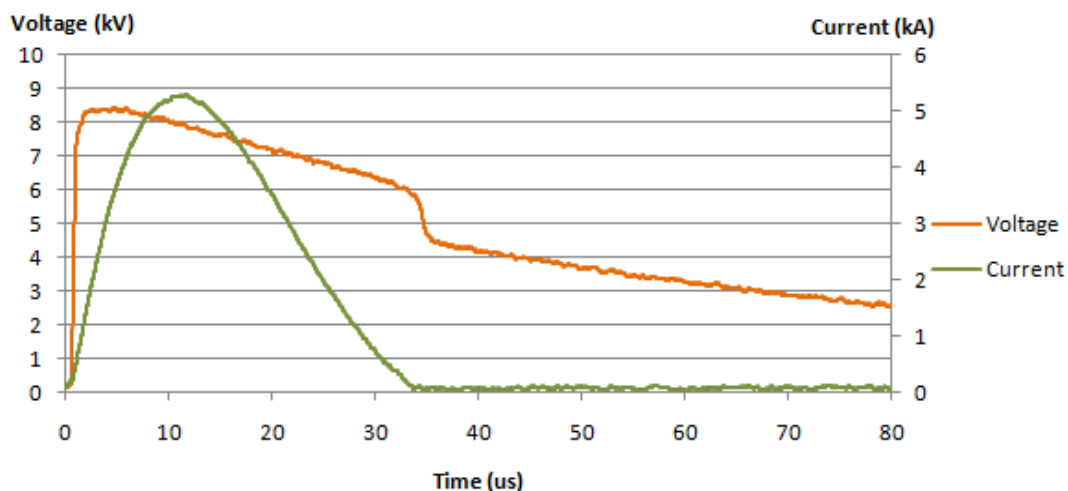


Figure 3.14 An example of Lightning Combination Oscillograms Used for Impulse Degradation

3.2.4.2 Heat Degradation

As can be referred back in Table 3.2, samples B (block-type) and D (radial leaded-type) were systematically subjected to three levels of laboratory heat degradation. For each degradation level, the samples were preheated at 120°C for five days. Then, prior to any diagnostic measurements, the varistors were cooled down at room temperature. The heat degradation experiment was conducted by using a laboratory oven, NAILIK Digimatic Drying Oven, as shown in Figure 3.15. Temperature of the preheated varistors is controlled automatically by the drying oven temperature controller. The drying oven has the following specifications:

| | |
|---------------------|--------------------------------------|
| Manufacturer: | NAILIK Engineering |
| Model: | NL 1017-C |
| Capacity: | 120 litres |
| Internal Dimension: | 558 mm (H) x 490 mm (W) x 460 mm (D) |
| External Dimension: | 845 mm (H) x 600 mm (W) x 546 mm (D) |
| Power Rating: | 2000 W |
| Temperature Range: | 40°C - 200°C |
| Power Supply: | 240 V, 50 Hz |
| Weight: | 62 kg |



Figure 3.15 Digimatic Drying Oven

3.3 Interpretation of RVM

In order to gain exact information of the material insulation condition, data and results from RV measurements have to be interpreted reliably. In this project, the data and results from RVM were evaluated according to a successful interpretation approach for evaluation of transformer [17] and cable [6, 16] insulation system, which is based on new ageing parameter, *p-factor*.

On the basis of return voltage, U_r , equation obtained from the analysis of return voltage phenomenon in Figure 3.3 and under the assumption that measurement system resistance is very large compared to the resistors R_1 and R_2 , three common basic parameters used in evaluation of RVM results can be calculated analytically [29]. These parameters, namely, the maximum RV, U_m , the time to maximum RV, t_m and the initial slope of RV, s , are given as follows,

$$U_m = U_s \left(\lambda^{\frac{1}{1-\lambda}} - \lambda^{\frac{\lambda}{1-\lambda}} \right)$$

$$s = \frac{U_s}{\tau_1} \left(\frac{\lambda - 1}{\lambda} \right)$$

$$t_m = \tau_1 \left(\frac{\lambda}{\lambda - 1} \right) \ln \lambda$$

Obviously, the diagnostic parameters U_m and s contain the complex factor of U_s and dielectric constants ratio, $\lambda = \tau_1/\tau_2$ and consequently, influenced by the geometric dimensions of the test object. The time t_m of the maximum RV depends on dielectric constant, τ_1 and the dielectric constants ratio λ . From these three diagnostic parameters, a new parameter, *p-factor*, is defined as [20],

$$p = \frac{U_m}{s t_m} = \frac{\lambda^{\frac{1}{1-\lambda}} - \lambda^{\frac{\lambda}{1-\lambda}}}{\ln \lambda}$$

The *p-factor* clearly eliminates the complex dependence on the factor U_s as well as U_p – since parameter s is inversely, and parameter t_m is proportionally related to parameter τ_1 . It is also independent from the geometric dimensions of the two

dielectrics and all parameter changes that influence τ_1 and τ_2 in the same way as the temperature. The *p-factor* is claimed to sensitively increase with ageing processes of the test object [20]. The relationship between *p-factor* and λ can be seen in Figure 3.16 and these two parameters were used to evaluate the condition of varistor insulation in this project.

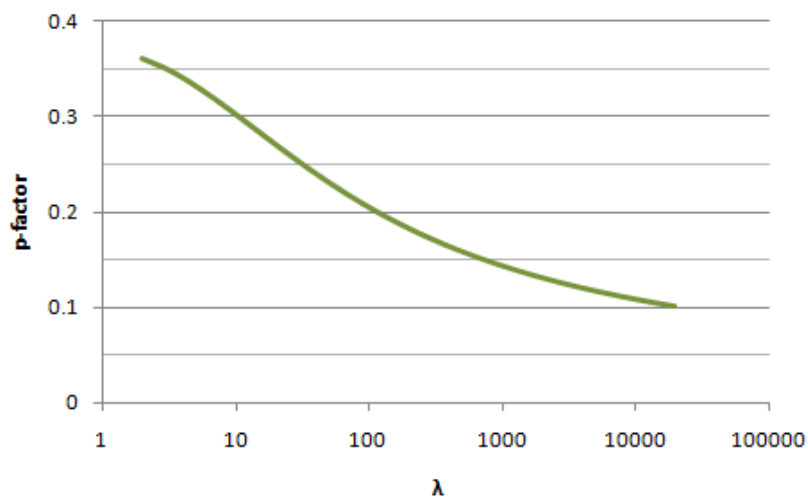


Figure 3.16 Relationship between *p-factor* and λ

3.4 Project Flow Chart

The methodology of the project can be summarized in a flow chart form as shown in Figure 3.17.

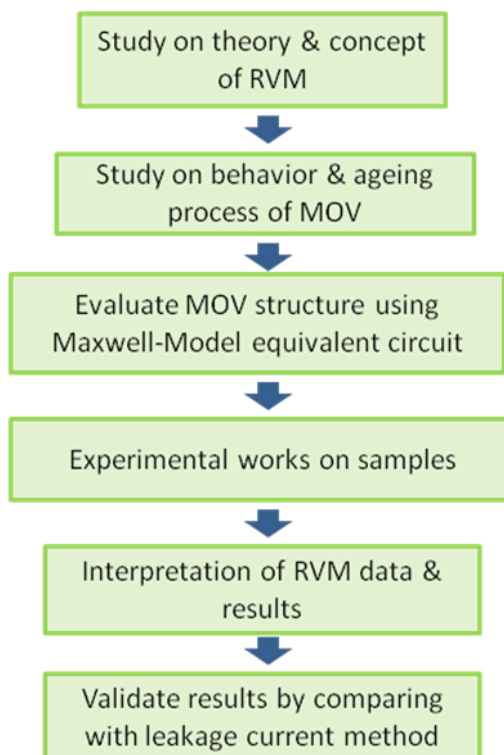


Figure 3.17 Flow Chart of Project

CHAPTER 4

DATA AND DISCUSSION

4.1 Introduction

The chapter presents detail RVM results as well as discussions for each sample. The analysis of the basic RVM parameters, U_m , t_m and s , and the new parameter, p -factor, are visualized in terms of graphical plots. For the total leakage current and 1 mA reference voltage measurements, the results are tabulated in tables which consists of the measurements data for each degradation level of each sample. All data from the RV, total leakage current and 1 mA reference measurements are tabulated in a single table for comparison of the techniques' sensitiveness.

4.2 Results of Return Voltage Measurements

4.2.1 Sample A – Impulse Degradation

The measurements were carried out before and after each degradation level described in Table 3.2 using the experimental setup shown in Figure 3.6. Figure 4.1 shows the plots of RVM essential parameters – peak of RV, initial slope of RV and time-to-peak RV – of sample A after each degradation level. By referring to the figure, the values of U_m and t_m decrease after each degradation level. This indicates that the insulation condition of the varistor has changed and suggests the reduction of

its resistivity [13, 14]. Meanwhile, an increasing trend of s after each degradation level is an evidence of ageing processes in the varistor insulation [3].

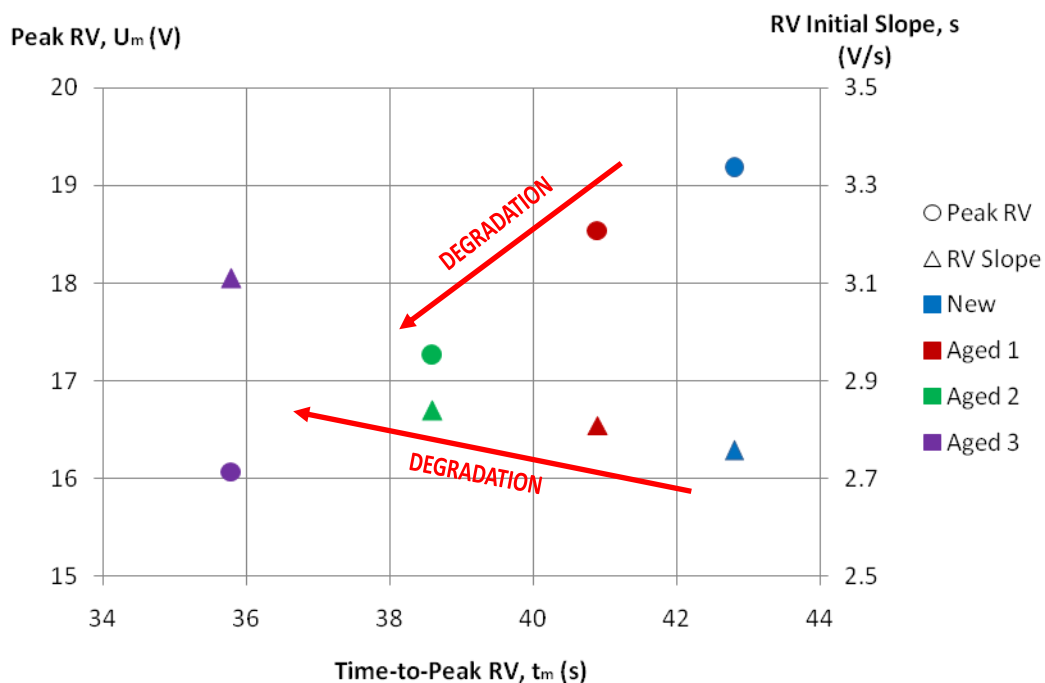


Figure 4.1 Peak RV, RV Initial Slope and Time-to-Peak RV Plots for Sample A

Based on the related equation as discussed in Section 3.3, the values of p -factor and λ can be calculated from the RVM parameters for each degradation level of the varistor. Figure 4.2 shows the relationship between p -factor and λ for sample A. It seems that the p -factor values decrease with degradation levels while the λ is increased. As can be seen in the figure, the value of λ is increased from about 420 for a new varistor to about 980 after it experienced three levels of degradation processes. It shows a contradiction to that from previous findings for cables insulation system whereby this relationship was in the opposite way [20, 30]. Nevertheless, this is an interesting finding as it agrees with previous researches on varistor microstructure in claiming that after ageing processes, the reduction of average grains size is much severe than the intergranular boundary [1, 10, 14]. In other words, the degradation processes of the varistor affect greater changes to its dielectric constant τ_1 compared to τ_2 resulting in the reduction of the p -factor values.

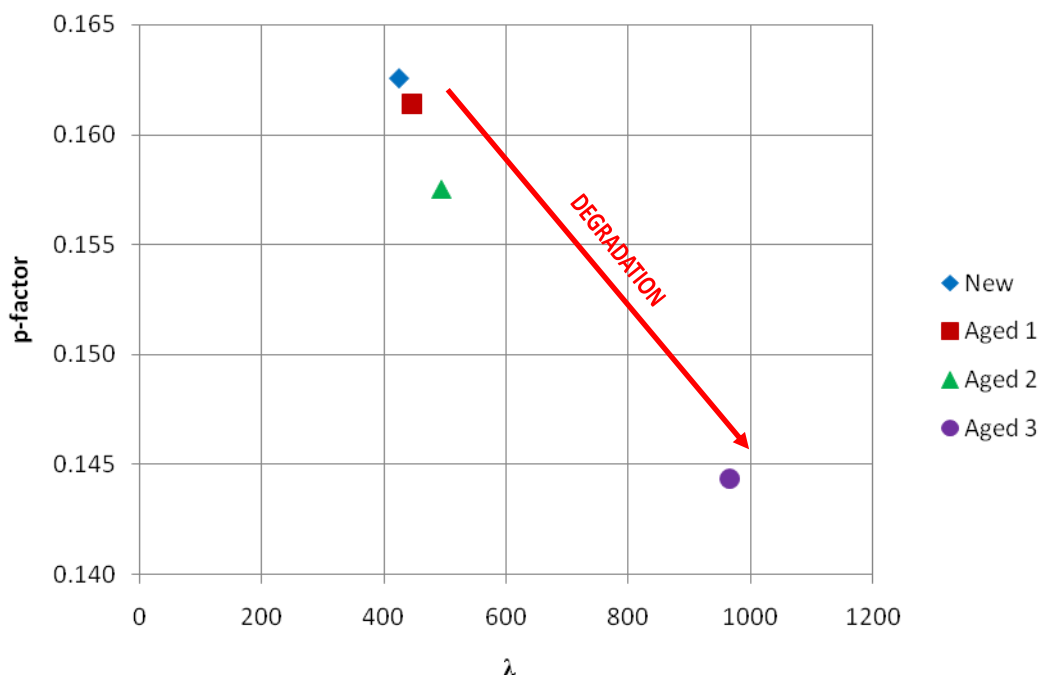


Figure 4.2 Relationship between p -factor and $\lambda = \tau_2/\tau_1$ for Sample A

4.2.2 Sample B – Heat Degradation

Sample B experienced three levels of heat degradation procedures as described in Table 3.2 and the three essential parameters of RVM were plotted in Figure 4.3. Based on the figure, U_m and t_m of the varistor decrease with levels of degradation as found in RVM results for sample A and this also suggests that the insulation condition of the varistor has changed due to the heat degradation processes. However, the changes of s is unexpected where it has a gradual decreasing trend from new condition to after two levels of degradation and then it shows an increment after the third level of degradation. For an aged varistor, the s value is claimed to increase with ageing processes due to an augmentation of polarization conductivity of the varistor [3].

For the p -factor evaluation of sample B, as can be referred in Figure 4.4, it seems that the value of the parameter shows a reduction from about 0.169 to 0.164

after the third level of degradation processes regardless on the values after the first and second degradation levels.

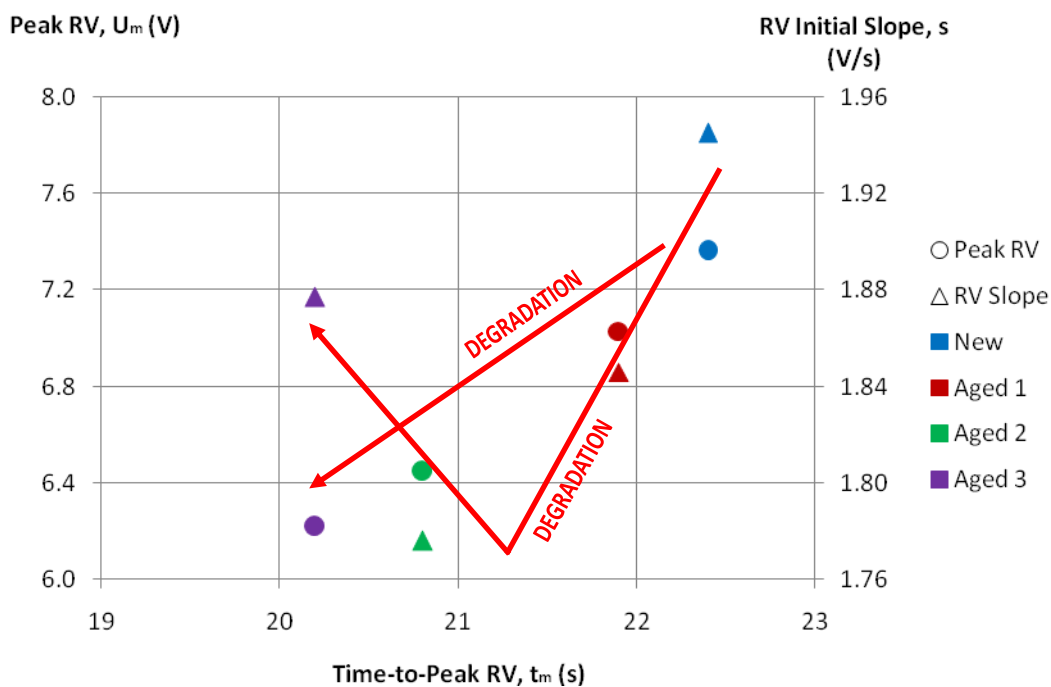


Figure 4.3 Peak RV, RV Initial Slope and Time-to-Peak RV Plots for Sample B

This finding suggests that after experiencing three levels of heat degradation, the characteristics of the varistor insulation have changed in a way that affects the dielectric time constants – τ_1 and τ_2 – of the varistor. An increment of the λ value after three levels of degradation show that the dielectric time constants of ZnO grains, τ_1 , experienced greater decrement as compared to the dielectric time constant of intergranular layers, τ_2 .

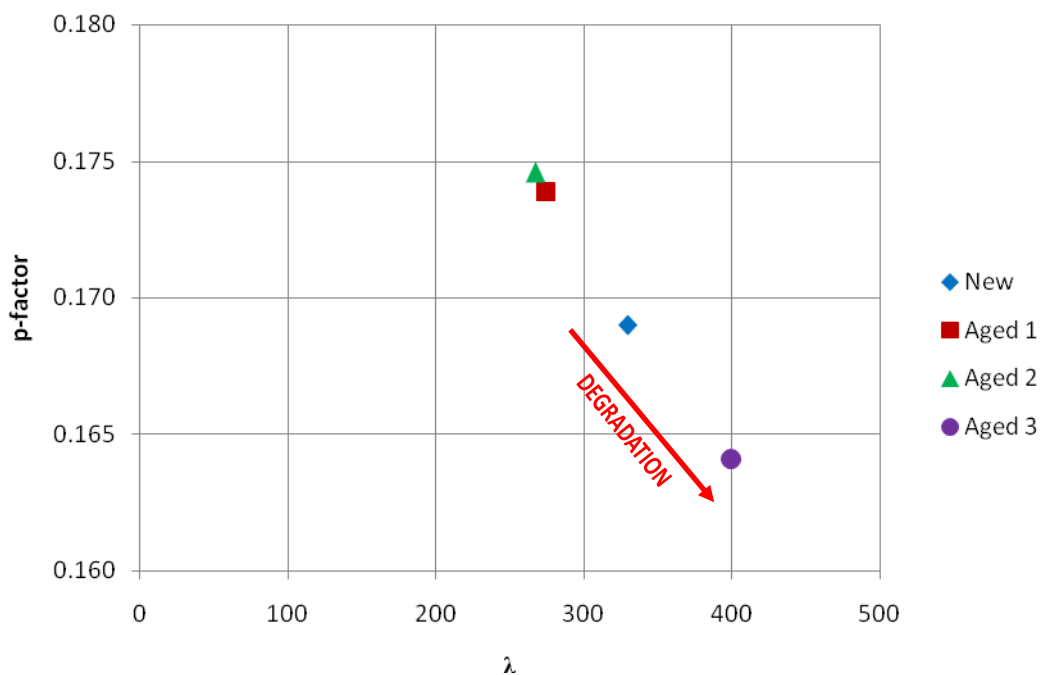


Figure 4.4 Relationship between p-factor and $\lambda = \tau_2/\tau_1$ for Sample B

4.2.3 Sample C – Impulse Degradation

The measurements were conducted before and after each degradation level of the sample as shown in Table 3.2. Plots of the RVM essential parameters can be seen in Figure 4.5. The figure shows the plots of the parameters for only up to the second degradation because the sample was failed after the third impulse degradation. Referring to the figure, there is no significant trend lies between U_m and s for each degradation process. Apart from that, the t_m values increase for all three degradation levels. These findings are inconsistent with the published works by Saha and Mardira [1, 13, 14]. Nevertheless, the relationship between *p-factor* and λ of the sample is explainable on the varistor ageing processes as shown in Figure 4.6.

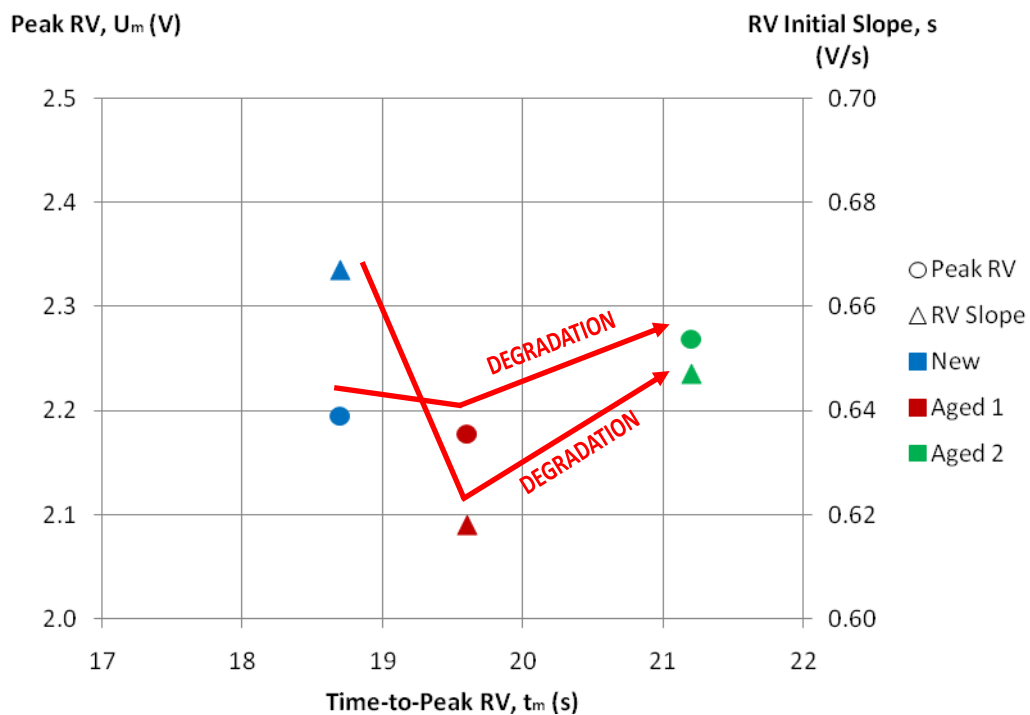


Figure 4.5 Peak RV, RV Initial Slope and Time-to-Peak RV Plots for Sample C

According to the figure, the value of p -factor decreases after it experienced two levels of impulse degradation resulting an increment in λ value. This signify that the dielectric constants of the varistor have changed due to the impulse subjection similar to the block-type sample (Sample A) as discussed in Section 4.2.1.

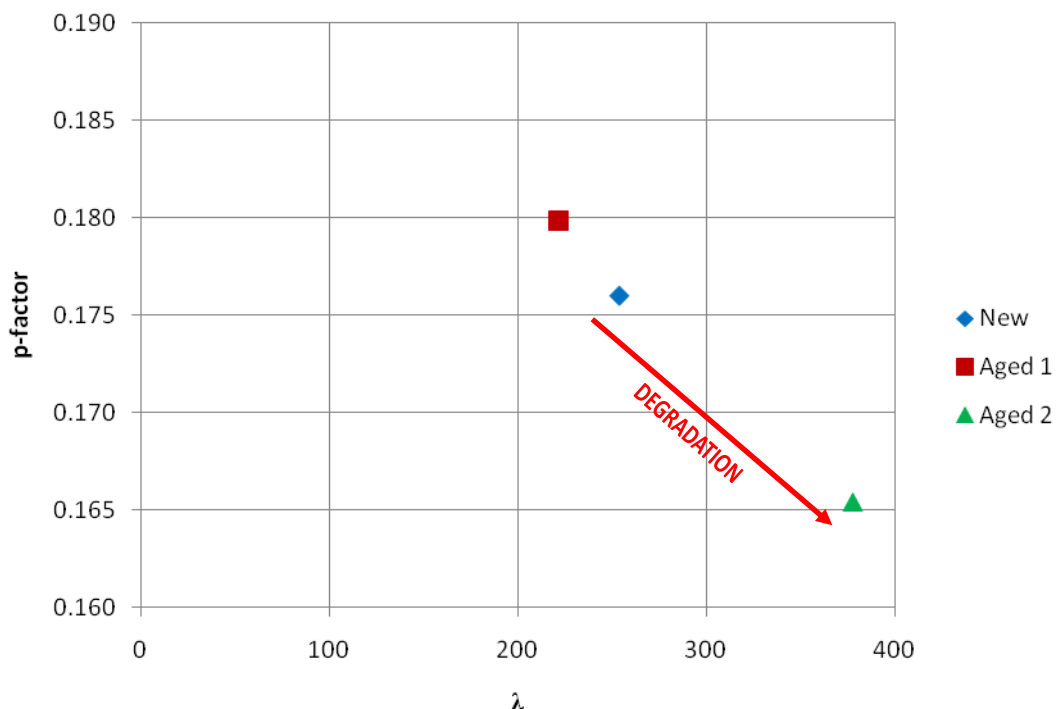


Figure 4.6 Relationship between p -factor and $\lambda = \tau_2/\tau_1$ for Sample C

4.2.4 Sample D – Heat Degradation

RV measurements of Sample D were also performed before and after three degradation levels; heat degradation technique. The results of essential RVM parameters are plotted and shown in Figure 4.7. Referring to the figure, there are some anomaly in the changes of the essential parameters where these parameter values show no substantial trend that consider the ageing processes in the varistor condition. However, based on the p -factor plots for each degradation level as shown in Figure 4.8, the value of p -factor decreases after the degradation processes except after the second degradation level. This implies that the degradation processes affected the varistor condition in terms of the changes in dielectric time constants of the ZnO grains and intergranular layers as discussed in previous samples.

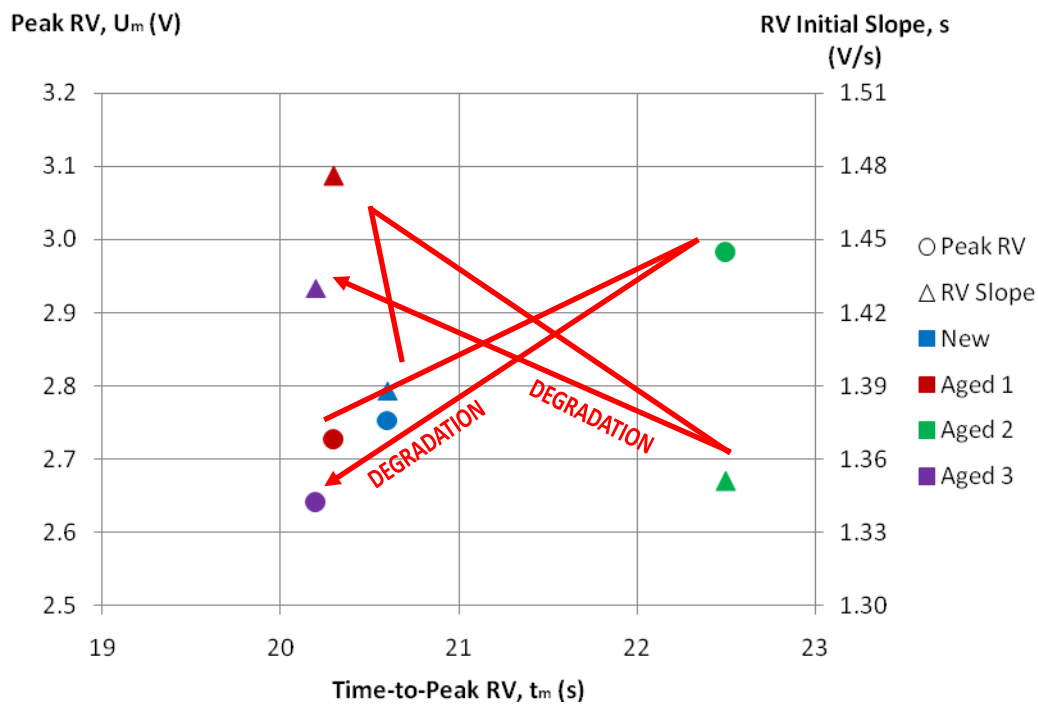


Figure 4.7 Peak RV, RV Initial Slope and Time-to-Peak RV Plots for Sample D

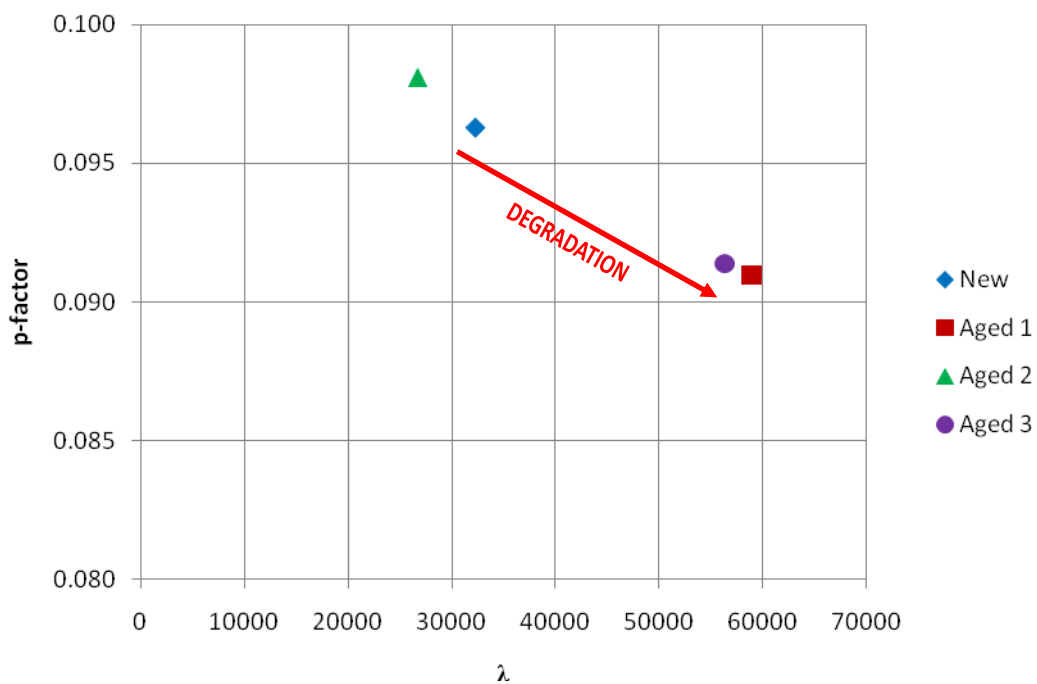


Figure 4.8 Relationship between p-factor and $\lambda = \tau_2/\tau_1$ for Sample D

4.3 Results of Total Leakage Current Measurements

The total leakage current measurements were carried out before and after each degradation for each sample. For each measurement, the rms value of the elevated applied voltage and the total leakage current correspond to this voltage were recorded and plotted as a linear relationship. Slope of the graph is used as a reference method for the RVM. Figure 4.9 shows the total leakage current graphs for sample D. Results for all measurements are summarized in Table 4.1 and are illustrated in Figure 4.10.

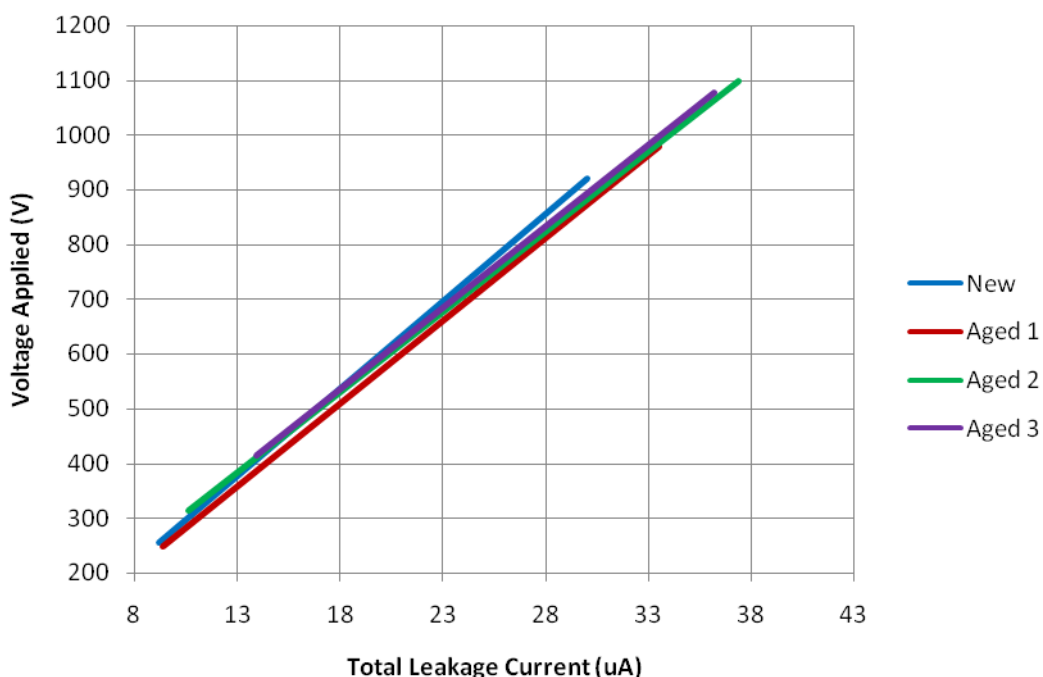


Figure 4.9 Total Leakage Current Measurements for Sample D

Referring to the table and the figure, the expected decrement trend in the slope of leakage current – due to reduction of applied voltage for same leakage current flowing through varistor – after each degradation level is not achieved except for sample C. The fluctuated values of the slope of total leakage current indicate that the technique contains no important information of the ageing processes of the varistors may be due to the dominant capacitive component in the leakage current [28]. For sample C, the gradual reduction of the total leakage current slope with

degradation processes suggests the varistor insulation condition change in a way that increase its conductivity before failed at the third degradation level.

Table 4.1 Results of Total Leakage Current Measurements

| Degradation Level | Slope of Total Leakage Current (V/ μ A) | | | |
|-------------------|---|----------|----------|----------|
| | Sample A | Sample B | Sample C | Sample D |
| New | 9.586 | 8.98 | 32.48 | 31.26 |
| 1 st | 8.973 | 8.99 | 30.2 | 29.75 |
| 2 nd | 9.089 | 8.93 | 27.52 | 28.97 |
| 3 rd | 9.472 | 8.97 | ~Failed~ | 29.46 |

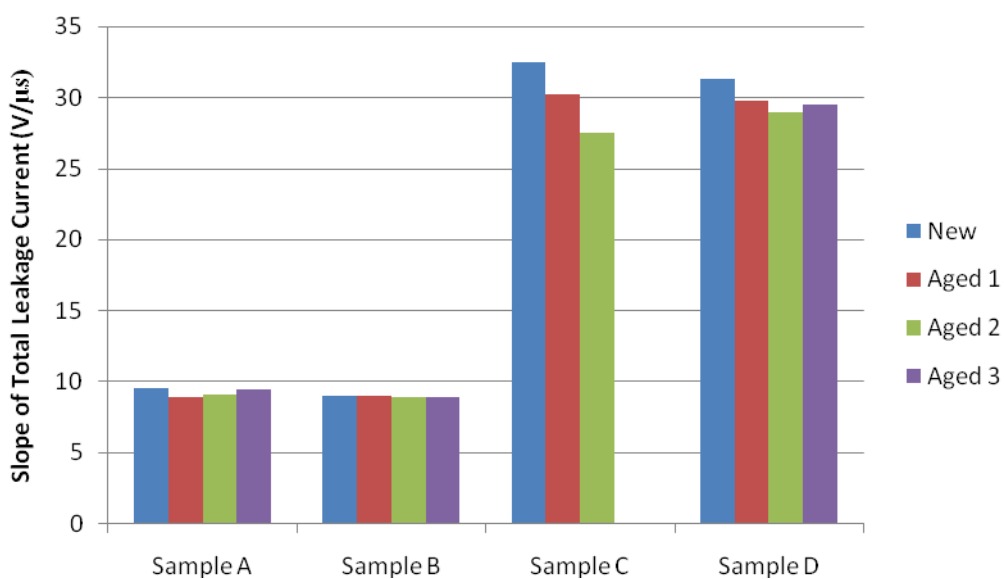


Figure 4.10 Chart of the Slope of Total Leakage Current Measurements for All Samples

4.4 1 mA Reference Voltage Measurements

As discussed earlier in Section 3.2.3, the reference voltage for 1 mA peak leakage current flowing through varistor is measured before and after each degradation level. Results of 1mA reference voltage for all sample are summarized in Table 4.2. Figure 4.11 illustrates the results from the table.

According to the table and the figure, they show that the 1 mA reference voltages reduce with degradation levels for all samples. This implies that the samples have experienced ageing processes after each degradation level which affected the resistivity of the samples to decrease [28]. Changes in the varistor condition due to the degradation processes lead to the reduction of the measured reference voltage.

Table 4.2 Results of 1 mA Reference Voltage Measurements

| Degradation Level | 1 mA Reference Voltage (kV) | | | |
|-------------------|-----------------------------|----------|----------|----------|
| | Sample A | Sample B | Sample C | Sample D |
| New | 4.058 | 3.998 | 1.531 | 1.516 |
| 1 st | 4.051 | 3.973 | 1.515 | 1.493 |
| 2 nd | 4.046 | 3.946 | 1.494 | 1.478 |
| 3 rd | 4.038 | 3.936 | ~Failed~ | 1.469 |

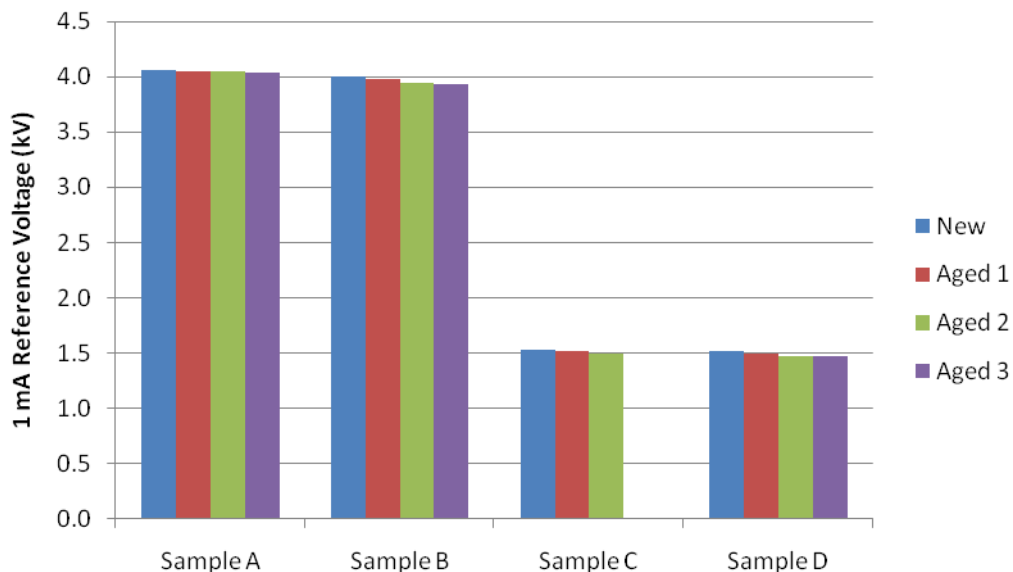


Figure 4.11 Chart of 1 mA Reference Voltage Measurements for All Samples

4.5 Results Comparison

All results for RVM, total leakage current and 1 mA reference voltage techniques are compiled in Table 4.3 in term of percentage of change which is calculated according to the equation,

$$\text{Percentage of Change (\%)} = \frac{X_{\text{after}} - X_{\text{before}}}{X_{\text{before}}} \times 100\%$$

where X_{before} is value of the parameter before degradation process and X_{after} represents the parameter's value after experiencing the degradation process. Figure 4.12 illustrates the percentage of changes between all techniques for all sample in a chart form.

By referring to the table and the figure, obviously, the RVM parameters (pink column) shows greatest changes compared to the total leakage current (yellow column) and 1mA reference voltage (green column) techniques. This observation may be an evidence of the RVM sensitiveness in detecting the changes in varistor condition as also proven by previous works [1, 3, 13].

Table 4.3 Results Comparison between RVM, Total Leakage Current and 1 mA Reference Voltage Techniques

| Sample | Degradation Level | % of Change | | | | | |
|--------|-------------------|-----------------------------|-------|------|----------|--------------------------------|-----------------------|
| | | Return Voltage Measurements | | | p-factor | Slope of Total Leakage Current | 1mA Reference Voltage |
| | | U_m | t_m | s | | | |
| A | 1 st | -3.3 | -4.4 | 1.9 | -0.7 | -6.4 | -0.2 |
| | 2 nd | -6.9 | -5.6 | 1.1 | -2.4 | 1.3 | -0.1 |
| | 3 rd | -6.9 | -7.3 | 9.5 | -8.4 | 4.2 | -0.2 |
| B | 1 st | -4.5 | -2.2 | -5.1 | 2.9 | 0.1 | -0.6 |
| | 2 nd | -8.3 | -5 | -3.8 | 0.4 | -0.7 | -0.7 |
| | 3 rd | -3.6 | -2.9 | 5.7 | -6.1 | 0.4 | -0.3 |
| C | 1 st | -0.8 | 4.8 | -7.3 | 2.2 | -7 | -1 |
| | 2 nd | 4.2 | 8.2 | 4.7 | -8 | -8.9 | -1.4 |
| | 3 rd | ~ Failed ~ | | | | | |
| D | 1 st | -1.2 | -1.5 | 6.3 | -5.5 | -4.8 | -1.5 |
| | 2 nd | 9.4 | 10.8 | -8.5 | 7.8 | -2.6 | -1 |
| | 3 rd | -11.5 | -10.2 | 5.8 | -6.8 | 1.7 | -0.6 |

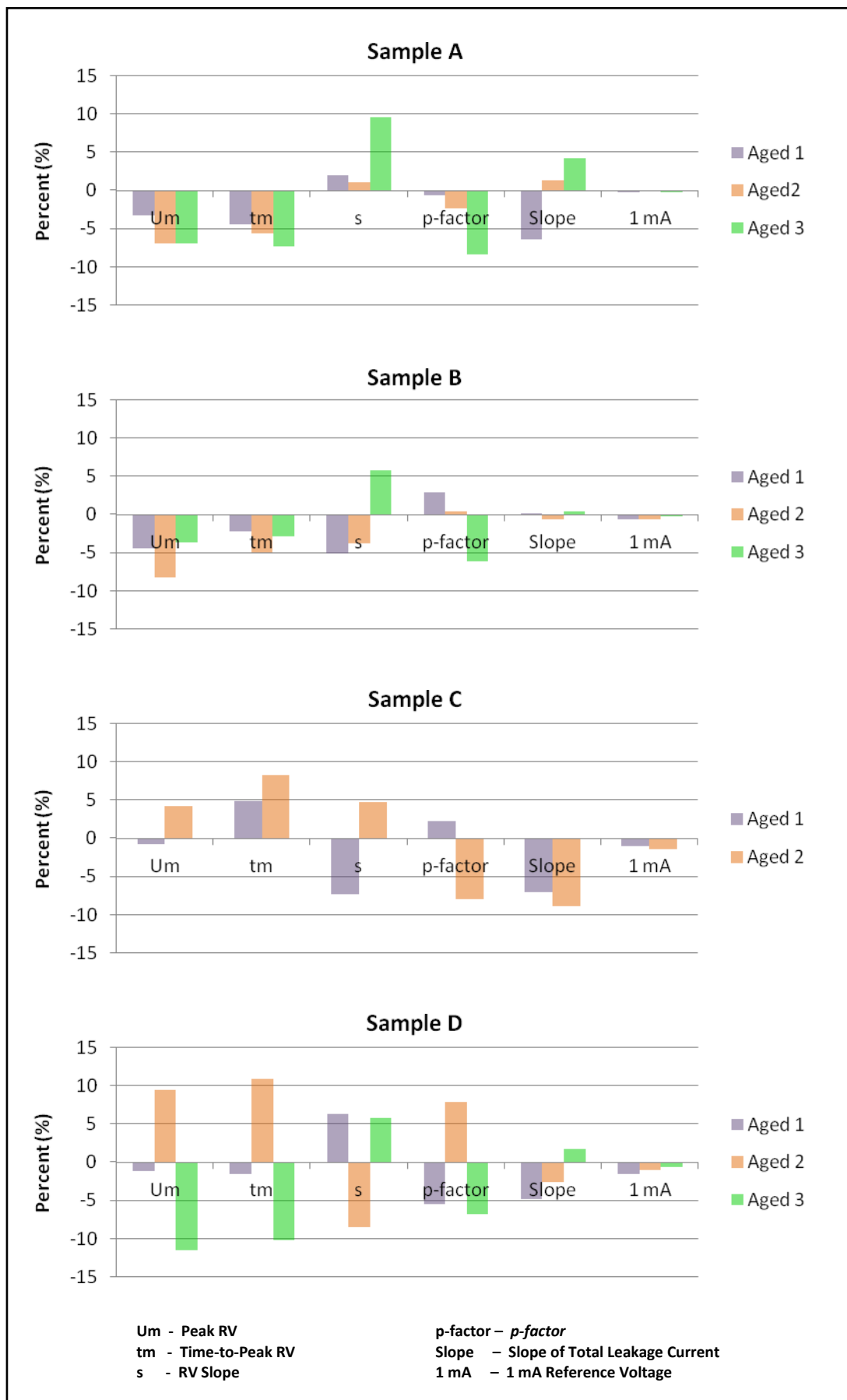


Figure 4.12 Charts of Results Comparison for Each Technique for all Samples

CHAPTER 5

CONCLUSION & SUGGESTION

5.1 Conclusion

The evaluation of RVM on MO varistors only on the basis of three essential parameters gives deficient information about the varistor insulation condition. The Maxwell-Model for multilayer dielectric seems to be an adequate equivalent circuit for MO microstructure in order to attain better information during the RV measurement phenomenon. The model provides the interpretation of RV parameters based on dielectric time constants which separately portray the microstructure condition of MO varistor. New ageing parameter, *p-factor*, obtained from the evaluation of the model solves the dependency on the measurement parameters such as t_c , t_d and sample temperature.

Evidently, from this work, the changes in *p-factor* and λ propose better information of ageing processes in the varistor microstructure - zinc oxide grains and intergranular layers – separately based on the changes in the dielectric time constants of both materials. The results also show that the *p-factor* parameter presents considerable correlation to the ageing processes regardless of the trend of the basic essential RVM parameters, namely, U_m , t_m and s .

Apart from that, the total leakage current measurement technique provides little information on the condition of MO varistor. Compared to the total leakage and

1mA reference voltage measurements, the results have shown that the RVM technique has a greater sensitivity in detecting the changes in microstructure of MO varistors. The RVM technique has therefore been proven as an efficient tool for the assessment of ageing processes of MO varistor.

5.2 Suggestion

More RVM studies on various types of MO varistors using various levels of degradation have to be done in order to obtain additional information of varistor condition as well as to determine the reliability of the interpretation technique. For degradation detection techniques, more accurate tests are required in order to gain information in the real ageing processes condition such as due to impulse degradation tests together with power frequency operating voltage, and et cetera. Comparison of the RVM technique with a well-known and accurate diagnostic technique, for instant, the pure resistive leakage current measurements, has to be done in order to obtain a specific ageing information on the varistor condition such as the degree of degradation.

REFERENCES

- [1] Mardira, K. P., Saha, T. K. and Sutton, R. A. The Effects of Electrical Degradation on the Microstructure of Metal Oxide Varistor. *Transmission and Distribution Conference and Exposition*. Oct 28–Nov 2, 2001. IEEE/PES. 2001. 329-334.
- [2] Vahe Der Houhanessian and Walter S. Zaengl. On-Site Diagnosis of Power Transformers by Means of Relaxation Current Measurements. *Conference Record of the 1998 International Symposium on Electrical Insulation*. June 7-10, 1998. Virginia, USA: IEEE. 1998. 28-34
- [3] Nemeth, E. Measuring Voltage Response: A Non-destructive Diagnostic Test Method of HV Insulation. *IEE Proceedings Science, Measurement and Technology*. Sept 1999: IEE. 1999. 249-252.
- [4] Saha, T. K. and Purkait, P. Investigation of Polarization and Depolarization Current Measurements for the Assessment of Oil-Paper Insulation of Aged Transformers. *IEEE Transactions on Dielectrics and Electrical Insulation*. Feb 2004. IEEE. 2004. 144-154.
- [5] Saha, T. K. and Dinh, T. Return Voltage Measurements on Metal Oxide Surge Arrester. *High Voltage Engineering Symposium*. August 22-27, 1999. IEE. 1999. 313-316.
- [6] Rainer, P. and Oleg, K. Return Voltage Measurements – The Step from Experimental Data to a Relevant Diagnostic Interpretation. *Proceedings of 2005 International Symposium on Electrical Insulating*. June 5-9, 2005. Japan: IEEE. 2005.
- [7] EPCOS. *SIOV Metal Oxide Varistor*. General Technical Information. Dec 2007.
- [8] Haddad, A. and Warne, D. *Advances in High Voltage Engineering*. London, United Kingdom. The Institution of Electrical Engineers. 2005.

- [9] Kazuo Eda. Zinc Oxide Varistor. *IEEE Insulation Magazine*. 1989. 5(6): 28-41.
- [10] Sargent, R. A., Darveniza and Dunlop, G. L. Effects of Multiple Current Pulses on the Microstructure and Electrical Properties of Zinc Oxide Varistor. *Proceedings of the 3rd International Conference on Properties and Applications of Dielectric Materials*. July 8-12, 1991. Tokyo: IEEE. 1991. 509-512.
- [11] Vipin, P. M., Nagabhushana, G. R. and Jayaram B. N. Investigations on Electro-Thermal Ageing of Metal Oxide Surge Arrester Elements: A Realistic Laboratory Simulation. *Proceedings of The 3rd International Conference on Properties and Applications of Dielectric Materials*. July 8-12, 1991. Tokyo: IEEE. 1991. 1152-1155.
- [12] Muhridza, Y. M. *The Behaviour and Performance of Metal Oxide Varistor Under the Application of Multiple Lightning Impulses*. PhD Thesis. Universiti Teknologi Malaysia; 2005.
- [13] Mardira, K. P. and Saha, T. K. Modern Electrical Diagnostics for Metal Oxide Surge Arrester. *Transmission and Distribution Conference and Exhibition*. 6-10 Oct. 2002. Asia Pacific: IEEE/PES. 2002. 672-676.
- [14] Mardira, K. P., Saha, T. K. and Sutton, R. A. Investigation of Diagnostic Technique for Metal Oxide Surge Arresters. *IEEE Transactions on Dielectrics and Electrical Insulation*. Feb 2005. IEEE. 2005. 50-59.
- [15] Nouruddeen Bashir and Hussein Ahmad. Diagnosis of XLPE Cable using the Recovery Voltage Measurement Method. *The 5th Student Conference on Research and Development*. Dec 11-12, 2007. Malaysia: IEEE. 2007. 1-4.
- [16] Rainer Patsch and Oleg Kouzmine. Return Voltage Measurements – a Good Tool for the Diagnosis of Paper-Oil Insulations. *Power Tech, 2005*. June 27-30, 2005. Russia: IEEE. 2005.
- [17] Patsch, P. and Menzel, J. Ageing and Degradation of Power Transformers – How to Interpret Return Voltage Measurements. *Proceedings of 2008 International Symposium on Electrical Insulating Materials*. Sep 7-11, 2008. Yokkaichi, Japan: IEEE. 2008. 179-182.
- [18] J. P. van Bolhuis, E. Gulski, G. M. Urbani and H. F. A. Verhaart. Development of Knowledge Rules of RVM for Interpretation of the Condition of Transformer Insulation. *Conference Record of the 2000 IEEE International*

- Symposium on Electrical Insulation*. April 2-5, 2000. Anaheim, USA: IEEE. 2000. 267-270.
- [19] Pastch, R. and Kouzmine, O. The Influence of Climatic Conditions on the Diagnostics Results of Return Voltage Measurements. *Conference Record of the 2002 IEEE International Symposium on Electrical Insulation*. April 7-10, 2002. Boston, USA: IEEE. 2002. 191-194.
- [20] Rainer Patsch and Oleg Kouzmine. p-Factor, a Meaningful Parameter for the Evaluation of Return Voltage Measurements. *2002 Annual Report Conference on Electrical Insulation and Dielectric Phenomena*. IEEE. 2002. 906-909.
- [21] Saha, T. K. and Mardira, K. P. Modeling Metal Oxide Surge Arrester for the Modern Polarization Based Diagnostics. *IEEE Transactions on Dielectrics and Electrical Insulation*. Dec 2005. IEEE. 1249-1258.
- [22] K. Ragaller. *Surges in High Voltage Networks*. New York: Plenum Press. 1979.
- [23] Patsch, R., Jung, J. and Kouzmine, O. The Interpretation of Return Voltage Curves of Paper-Oil Cables. *Annual Report Conference on Electrical Insulation and Dielectric Phenomena*. Oct 2000. IEEE. 2000.39-42.
- [24] Patsch, R and Jung, J. Improvement of the Return Voltage Method for Water Tree Detection in XLPE Cables. *Conference Record of the 2000 IEEE International Symposium on Electrical Insulation*. April 2-5, 2000. USA: IEEE. 2000. 133-136.
- [25] B. Tareev. *Physics of Dielectric Materials*. First Edition. Moscow: Mir Publishers. 1975.
- [26] International Electrotechnical Commission. *Surge Arresters Part 4: Metal Oxide Surge Arrester without Gaps for AC Systems*. IEC 60099-4. 1998.
- [27] Institute of Electrical and Electronics Engineers. *IEEE Standard for Metal-Oxide Surge Arresters for AC Power Circuits (>1 kV)*. IEEE Std C62.11. 2005.
- [28] Christodoulou, C. A., Avgerinos, M. V., Ekonomou, L., Gonos, I. F. and Stathopoulos, I. A. Measurement of the Resistive Leakage Current in Surge Arresters Under Artificial Rain Test and Impulse Voltage Subjection. *IET Science, Measurement and Technology* 2009. 2009. 3(3): 256-262.
- [29] Böning, P. Bemerkenswerte Zusammenhänge zwischen den anomalen Strömen, dem Verlustfaktor, der scheinbaren Kapazität und der Rückspannung bei Isolierstoffen. *Z. f. techn. Physik*. Nr. 8. 1938.

- [30] Patsch, R. and Kamenka, D. Return Voltage Measurements – Diagnostic Interpretations on the Basis of the Dielectric Time Constants. *APTADM 2007*. Wroclaw, Poland. 2007.
- [31] Lightning Eliminators & Consultant. *Improved Metal Oxide Varistor Packaging Technology for Transient Voltage Surge Suppressor*. Colorado, USA: LEC. 2003.

APPENDIX A

Block-type Varistor Specifications

Technical Data of Typical ZnO Varistors

Date: Jun. 19, 2009

| No | Description | 3kV/5kA | 4.5kV/5kA | 3kV/10kA | 4.5kV/10kA A | 3kV/10kA class 2 | 3kV/10kA class 3 | 3kV/10kA class 3 | 3kV/10kA class 3 | 3kV/10kA class 3 | 3kV/10kA class 4 |
|----|---|---------------------------------------|--|---------------------------------------|--|---------------------------------------|---------------------------------------|---------------------------------------|---------------------------------------|---------------------------------------|---------------------------------------|
| 1 | Rated voltage, kV | 3 | 4.5 | 3 | 4.5 | 3 | 3 | 3 | 3 | 3 | 3 |
| 2 | MCOV, kV | 2.55 | 3.6 | 2.55 | 3.6 | 2.55 | 2.55 | 2.55 | 2.55 | 2.55 | 2.55 |
| 3 | Lightning impulse (8/20) residual voltage, kV: - 5kA - 10kA - 20kA | 8.5 9.6 10.8 | 12.5 13.5 14.6 | 8.3 8.8 10.3 | 12.0 13.0 14.0 | 8.2 8.5 10 | 8.2 8.5 10 | 8.2 8.5 10 | 8.0 8.8 9.8 | 8.0 8.8 9.8 | 7.8 8.6 9.5 |
| 4 | Switch impulse (30/60), kV: - 125A - 500A | 7.2 8.0 | 10.6 11.7 | 7.0 7.8 | 10.5 11.5 | 7.0 7.8 | 7.0 7.8 | 7.0 7.8 | 7.0 7.8 | 7.0 7.8 | 7.0 7.8 |
| 5 | Reference voltage, kV | >=3 | >=3 | >=3 | >=3 | >=3 | >=3 | >=3 | >=3 | >=3 | >=3 |
| 6 | Long duration, us | 2000 | 2000 | 2000 | 2000 | 2000 | 2000 | 2000 | 2000 | 2000 | 2000 |
| 7 | Steep current residual voltage, kV | 9.8 | 14.3 | 10.2 | 14.5 | 10 | 10 | 10 | 9.8 | 9.8 | 9.6 |
| 8 | KCT value for operation duty test: <= High current impulse, kA | 1.1 65 | 1.1 65 | 1.0 95 | 1.0 90 | 1.0 100 | 1.0 100 | 1.0 100 | 1.0 100 | 1.0 100 | 1.0 100 |
| 9 | Temporary over voltage, kV: - 0.1s - 1s - 10s - 100s - 1000s - 10000s | 3.6 3.5 3.3 3.15 3 2.7 | 5.4 5.25 4.95 4.73 4.5 4.05 | 3.6 3.5 3.3 3.15 3 2.7 | 5.4 5.25 4.95 4.73 4.5 4.05 | 3.6 3.5 3.3 3.15 3 2.7 | 3.6 3.5 3.3 3.15 3 2.7 | 3.6 3.5 3.3 3.15 3 2.7 | 3.6 3.5 3.3 3.15 3 2.7 | 3.6 3.5 3.3 3.15 3 2.7 | 3.6 3.5 3.3 3.15 3 2.7 |
| 10 | 2ms rectangular current, A | 130 | 130 | 250 | 250 | 500 | 600 | 800 | 1000 | 1200 | |
| 11 | Dimension, mm | Dia 32x21 | Dia 32x31 | Dia 40x21 Dia 42 x21 | Dia 40x31 Dia 42x31 | Dia 56x21 | Dia 63x21 | Dia 70x21 | Outer Dia 72x21 Inner Dia 26mm | Outer Dia 80x21 Inner Dia 26mm | |

APPENDIX B

Radial Leaded-type Varistor Specifications

LITTELFUSE - V1000LA80AP - VARISTOR, 1000VAC



Image is for illustrative purposes only. Please refer to product description

Manufacturer: LITTELFUSE

Order Code: 1463590

Manufacturer Part No: V1000LA80AP

RoHS : ● Yes

Description

- VARISTOR, 1000VAC
- Series:LA
- Voltage Rating, AC:1000V
- Suppressor Type:Varistor
- Voltage Rating, DC:1200V
- Peak Pulse Current IPP @ 8/20µs:4500A
- Voltage, Clamping 8/20µs Max:2700V
- Max Transient Energy 10/1000µs:220J
- Capacitance:130pF
- Termination Type:Radial Leaded
- Case Style:Radial
- Transient Energy:220J
- Voltage, Clamping Max:2700V
- Voltage, Varistor:1000V
- Voltage, Varistor at 1mA Max:1800V
- Voltage, Varistor at 1mA Min:1425V

APPENDIX C

Printed Results from RVM 5462

```

-----
- Proc (CrvRec):
MOV TEST
- Identifier:
BLOCK A AGED1 2
- Comment:
No comment

```

```

Um = 500V
t = 27C
2009.08.27. 17:19

```

```

-----
Noise results (in 6s):
0.070 Upeak
0.001 U/s
0.017 Upp

```

```

.....
17:30:58
600.0s / 60.00s
20.26V
45.2s
2.375V/s
.....

```

```

-----
- Proc (CrvRec):
MOV TEST
- Identifier:
BLOCK B AGED2 1
- Comment:
No comment

```

```

Um = 500V
t = 27C
2009.08.27. 16:10

```

```

-----
Noise results (in 6s):
0.098 Upeak
0.010 U/s
0.018 Upp

```

```

.....
16:21:52
600.0s / 60.00s
7.671V
22.6s
2.052V/s
.....

```